# Elemental Geochemistry of Sedimentary Rocks at Yellowknife Bay, Gale Crater, Mars

**Article** · December 2013

DOI: 10.1126/science.1244734



**442 authors**, including:

John Bridges
University of Leicester
**297** PUBLICATIONS **7,256** CITATIONS

SEE PROFILE

Fred Calef
California Institute of Technology
**83** PUBLICATIONS **3,553** CITATIONS

SEE PROFILE

Pamela Conrad
NASA
**179** PUBLICATIONS **6,542** CITATIONS

SEE PROFILE

Sciencexpress Research Articles

# Elemental Geochemistry of Sedimentary Rocks at Yellowknife Bay, Gale Crater, Mars

S. M. McLennan,[1]* R. B. Anderson,[2] J. F. Bell III,[3] J. C. Bridges,[4] F. Calef III,[5] J. L. Campbell,[6] B. C. Clark,[7] S. Clegg,[8] P. Conrad,[9] A. Cousin,[8] D. J. Des Marais,[10] G. Dromart,[11] M. D. Dyar,[12] L. A. Edgar,[3] B. L. Ehlmann,[5,13] C. Fabre,[14] O. Forni,[15] O. Gasnault,[15] R. Gellert,[6] S. Gordon,[16] J. A. Grant,[17] J. P. Grotzinger,[13] S. Gupta,[18] K. E. Herkenhoff,[2] J. A. Hurowitz,[1] P. L. King,[19] S. Le Mouélic,[20] L. A. Leshin,[21] R. Léveillé,[22] K. W. Lewis,[23] N. Mangold,[20] S. Maurice,[24] D. W. Ming,[25] R. V. Morris,[25] M. Nachon,[20] H. E. Newsom,[16] A. M. Ollila,[16] G. M. Perrett,[6] M. S. Rice,[13] M. E. Schmidt,[26] S. P. Schwenzer,[27] K. Stack,[13] E. M. Stolper,[13] D. Y. Sumner,[28] A. H. Treiman,[29] S. VanBommel,[6] D. T. Vaniman,[30] A. Vasavada,[5] R. C. Wiens,[31] R. A. Yingst,[30] MSL Science Team†

*Corresponding author. E-mail: Scott.McLennan@stonybrook.edu

†MSL Science Team authors and affiliations are listed in the supplementary materials.

Author affiliations are shown at the end of the text.

**Sedimentary rocks examined by the Curiosity rover at Yellowknife Bay, Mars, were derived from sources that evolved from approximately average Martian crustal composition to one influenced by alkaline basalts. No evidence of chemical weathering is preserved indicating arid, possibly cold, paleoclimates and rapid erosion/deposition. Absence of predicted geochemical variations indicates that magnetite and phyllosilicates formed by diagenesis under low temperature, circum-neutral pH, rock-dominated aqueous conditions. High spatial resolution analyses of diagenetic features, including concretions, raised ridges and fractures, indicate that they are composed of iron- and halogen-rich components, magnesium-iron-chlorine-rich components, and hydrated calcium-sulfates, respectively. Composition of a cross-cutting dike-like feature is consistent with sedimentary intrusion. Geochemistry of these sedimentary rocks provides further evidence for diverse depositional and diagenetic sedimentary environments during the early history of Mars.**

Shortly after leaving its landing site at Bradbury Landing in Gale Crater, the Mars Science Laboratory Curiosity rover traversed to Yellowknife Bay (*1*), where it encountered a flat-lying, ~5.2-m-thick succession of weakly indurated clastic sedimentary rocks ranging from mudstones at the base to mainly sandstones at the top (*2*). Stratigraphic relationships and sedimentary structures indicate that this coarsening-upward succession likely represents sedimentation in an ancient fluvio-lacustrine system that would have been habitable. Also preserved is a spectrum of diagenetic features, including concretions, void spaces with a variety of sizes, geometries and origins, early diagenetic fractures ("raised ridges") filled with banded (possibly silicate) cements, possible sedimentary dikes, and a later diagenetic fracture system filled with sulfate cements, all indicating extended post-depositional aqueous fluid flow through the rocks (*2*).

Curiosity fully applied its analytical payload to investigate these sedimentary rocks and determine lithological, textural, chemical, mineralogical and isotopic compositions and their stratigraphic relationships (*2–4*). The payload of Curiosity includes two instruments capable of measuring elemental abundances. The alpha particle x-ray spectrometer (APXS) determines abundances on ~2.25 $cm^2$ surfaces and, when used in conjunction with the dust removal tool (DRT) or drilling system, can analyze relatively clean surfaces and drill cuttings. The laser-induced breakdown spectrometer (LIBS), part of the ChemCam remote sensing suite, detects atomic emission spectra from areas of ~0.1-0.3 $mm^2$ (depending on standoff distance), >2 orders of magnitude smaller than APXS. LIBS offers the additional capability of laser depth profiling (including surface dust removal) of up to ~1000 μm. These instruments provide complementary data by revealing both bulk rock compositions and compositions that can be related directly to textural features.

On Earth, the elemental geochemistry of clastic sedimentary rocks provides information central to interpreting sedimentary history, including chemical weathering history, nature and composition of the sediment provenance, sediment transport, and diagenetic history (*5–10*). In turn, geochemical understanding of these issues constrains many fundamental geological questions such as paleoclimates, tectonic relationships, basin evolution, diagenetic fluid flow and even crust-mantle evolution (*7*, *11–15*). Experience from the Mars Exploration Rovers Spirit and Opportunity, orbital spectroscopy and experiments using Mars-like compositions shows that such approaches are applicable to sedimentary environments on Mars where primary igneous compositions and aqueous conditions may differ from our terrestrial experience (*12*, *16–24*). Accordingly, we report elemental geochemistry of the ancient sedimentary rock succession, including its diagenetic features, preserved within Yellowknife Bay, evaluate these compositions in terms of the sedimentary history of this habitable paleoenvironment within Gale Crater and place them within the context of Martian surface environments early in the planet's history.

## Yellowknife Bay Stratigraphy

The geology, stratigraphy, sedimentology, and diagenetic history of Yellowknife Bay are described elsewhere (*2*). The sedimentary sequence, informally named the Yellowknife Bay formation, is subdivided into three members (Fig. 1) that likely were deposited in a prograding alluvial fan fluvio-lacustrine depositional system and influenced by at least two distinct diagenetic events. The formation is likely Hesperian in age but poorly constrained and could lie anywhere between early Hesperian (~3.7-3.4 Ga), if part of the early Gale Crater fill, to late Hesperian or early Amazonian (~3.4-1.5 Ga), if coeval with the nearby Peace Vallis alluvial fan exposed in Gale Crater (*2*).

The stratigraphically lowest Sheepbed member (>1.5 m thick), whose base is not exposed, is composed of gray-colored, bedded mudstone. Fine-grained texture, laterally extensive decimeter-scale bedding and stratigraphic relationships indicate deposition from suspension, likely in a distal alluvial fan lacustrine (or less likely playa) environment but possibly as ash fall. Early diagenetic textures, forming prior to or during

lithification, include millimeter-scale nodules interpreted as concretions, millimeter-scale rimmed "hollow nodules" interpreted as void space possibly formed by gas expulsion during early diagenesis, and narrow centimeter-sized intersecting "raised ridges," laterally correlative to nodules and hollow nodules, possessing resistant isopachous cements lining ridge margins, and interpreted as diagenetic cracks formed in early lithified sediment probably by reactions involving pore fluids [see figures 6, A to C, and 7 in (*2*)]. The upper ~50-75 centimeters of the Sheepbed member weathers more recessively than underlying beds and possesses higher abundances of both early and late diagenetic features. For geochemistry, we further subdivided the Sheepbed member into lower and upper parts with the boundary ~30 centimeters beneath the Gillespie Lake member in order to evaluate compositional transitions into the overlying stratigraphic unit.

The ~2.0 m thick Gillespie Lake member overlies the Sheepbed member with a sharp, likely erosional, contact. It consists of thin to medium bedded medium- to very coarse-grained sandstones with relict centimeter-scale cross-bedding. Mars Hand Lens Imager (MAHLI) and ChemCam Remote Micro-Imager (RMI) images indicate textural immaturity and compositionally diverse grains [see figure 5D in (*2*)]. This member was likely deposited in a distal fluvial environment. Gillespie Lake sandstones exhibit little primary porosity, suggesting a cemented rock, but may contain secondary porosity in the form of dispersed millimeter-scale vugs that may result from leaching of detrital grains or early diagenetic phases during fluid circulation or perhaps selective loss of readily degraded mudstone intraclasts during weathering (*2*). The Sheepbed (including early diagenetic features) and Gillespie Lake members are both cross-cut by a network of later diagenetic (post-lithification) intersecting fractures of variable thickness (hairline to ~8 mm) filled with light-toned cement, identified as Ca-sulfate by a variety of measurements (see below). These filled fractures are most abundant within the uppermost Sheepbed and the bright cements also fill hollow nodules where they intersect with fractures. Also cross-cutting the upper Sheepbed member is a ~8 centimeter wide dike-like feature termed the "snake," that terminates in a small anticline within the middle Gillespie Lake member, and is interpreted as a sedimentary dike injected due to high pore pressures that developed during rapid burial (*2*). A detailed 1.5 m stratigraphic section, termed the Selwyn Section, was measured across the Sheepbed–Gillespie Lake contact (Fig. 1 and fig. S1).

The upper Glenelg member (~1.7 m thick) is lithologically heterogeneous (*2*). The lower ~40 centimeters (e.g., Point Lake outcrop) is poorly understood but notable in possessing abundant millimeter- to centimeter-scaled voids. Possible interpretations include a debris flow, volcaniclastic layer, gas-charged sedimentary sill, perhaps related to the "snake," or a vesicle-rich volcanic flow (although there is no evidence for a nearby contemporaneous volcanic source). Some voids and cross-cutting fractures are filled with light-toned minerals, identified as Ca-sulfate by ChemCam, reminiscent of fracture fillings in the Sheepbed and Gillespie Lake members. We assume this part of the Glenelg is also sedimentary but are mindful of this uncertainty. The upper part of the Glenelg member (e.g., Shaler outcrop) consists of commonly cross-bedded interstratified sandstones and recessive finer grained sediment and was likely deposited mainly by fluvial processes, with paleocurrents indicating a source derived from the direction of the crater rim. At the top of this member are discontinuous fine-grained beds (e.g., Bathurst Inlet), in some cases with distinctive chemical compositions and possibly with distinctive origins (see below).

**Mineralogical and Geochemical Constraints from CheMin and SAM**

Two locations within the upper Sheepbed member, corresponding to APXS targets John_Klein and Cumberland, were drilled, with recovered powders being sieved (<150 μm) and delivered to CheMin and SAM for x-ray diffraction analysis of mineralogy and chemical-isotopic measurements of evolved gases using gas chromatography, quadrupole mass spectrometry and tunable laser spectrometry (*3*, *4*). Unsurprisingly for clastic sediments, both samples are composed of nonequilibrium mineral assemblages including primary igneous and a variety of secondary phases, notable for a ~30-40% amorphous component (including allophane-like material) and ~20% trioctahedral phyllosilicates. The remaining crystalline mineralogy includes (in decreasing amount) plagioclase, pyroxene, magnetite, Ca-sulfate (anhydrite, bassanite), forsteritic olivine (John_Klein only), akaganeite, sanidine, pyrrhotite, and possibly (<1-2%) hematite, ilmenite, pyrite, quartz, and halite. The exact mineralogy of the trioctahedral phyllosilicates is not fully constrained but they consist of a ~10Å collapsed saponitic smectite in John_Klein and, in Cumberland, clay minerals with both ~10Å and ~13.2Å spacing, possibly reflecting poorly-formed vermiculite (lacking the 7Å peak) or a smectite with either an interlayer cation with high hydration energy (e.g., Mg) or metal-hydroxy-groups (i.e., incipient chlorite). SAM analyses are also consistent with smectite, sulfates, sulfides, Fe-oxides and further indicate oxychlorine compounds (e.g., chlorate and/or perchlorate). Both instruments indicate heterogeneous Fe- and S-redox states. Mass balance calculations provide estimates of the chemical compositions of the combined amorphous component plus phyllosilicates and remaining crystalline minerals and these compositions (*4*) are used below.

**Clastic Sedimentary Rocks**

Yellowknife Bay S- and Cl-free compositions (all on weight percent basis) determined by APXS (*25*) (tables S1 to S4) correspond to iron-rich basalt (i.e., $SiO_2$ mostly <48%; $FeO_T$ mostly >20%; MgO ≈ 8-10%; Ni ≈ 200-900 ppm). Alkalis are variable ($Na_2O+K_2O$ ≈ 3-6%; $K_2O/Na_2O$ ≈ 0.2-1.3). CaO is highly variable (≈5-25%) but values above ~7% correspond to high $SO_3$, indicative of elevated levels of Ca-sulfate. Typical for the Martian surface, both $SO_3$ and Cl are mostly elevated in APXS observations due in part to surface soil and dust contamination. On brushed surfaces, APXS measurements of $SO_3$ are as low as 0.9% (Werneke_Brush, the analysis on the brushed surface of the Werneke target) suggesting the sedimentary rocks may have no more than 1-2% $SO_3$ on average. On the other hand, Cl abundances are higher than in most Martian soils (*26*), reaching 1.9% and commonly leading to low S/Cl ratios. Elevated Cl abundances (≥1%) are likely a primary rock feature rather than resulting from soil/dust coatings, consistent with the presence of oxychlorine compounds, akaganeite and possibly halite (*3*, *4*). Up to 9% magnetite in the crystalline component of Sheepbed mudstone drill samples was detected by XRD (*4*). We cannot completely exclude the possibility that very fine-grained magnetite was delivered as part of the detrital load into a lake environment, but on balance geochemistry suggests magnetite is not detrital. For example there are no systematic relationships between $FeO_T$/MgO and $FeO_T$ that could be explained by magnetite variations, no evidence from XRD (*4*) for enrichments of other minerals that might be expected to form part of a heavy mineral suite (e.g., spinels) nor correlations with related structural elements of these minerals (e.g., Cr, Ti) and no geochemical evidence, from APXS or ChemCam, for detrital magnetite enrichments (e.g., Fe-enrichment) in immediately overlying Gillespie Lake sandstones where heavy minerals might be expected to concentrate even more. Absence of geochemical evidence for detrital magnetite is also consistent with deposition of the Sheepbed mudstones from suspension into a lake, where heavy mineral concentrations are unlikely (*2*, *4*). Thus, magnetite is most likely a diagenetic phase rather than a detrital component.

Geochemical relationships are well illustrated in ternary diagrams plotting mole fractions $Al_2O_3$–($CaO+Na_2O$)–$K_2O$ (or A-CN-K) and $Al_2O_3$–($CaO+Na_2O+K_2O$)–($FeO_T$+MgO) (or A-CNK-FM) (Fig. 2). On these diagrams igneous minerals plot on or below the plagioclase–K-feldspar (A-CN-K) and feldspar-FM (A-CNK-FM) joins whereas secondary clay minerals plot above (*27*). The Chemical Index of Alteration

(CIA), defined as 100*A/(A+C+N+K), reveals any chemical weathering history by quantifying the systematic loss of relatively mobile elements (i.e., Ca, Na, K) from silicate minerals, and the scale is plotted beside the A-CN-K diagrams. For mafic sources, CIA above ~40-45 in bulk sediment suggests some chemical weathering history and above ~50-55 provides fairly compelling evidence for open system weathering (*10*). ChemCam (Fig. 2, C and D) analyzed many more targets than APXS (Fig. 2, A and B), and given the strategy of using its greater spatial resolution to target textural features (e.g., veins, ridges, grains), more scatter is both expected and observed. Mission experience so far indicates a slight instrument bias with ChemCam data plotting at higher $Al_2O_3$ on these diagrams than APXS, especially for alkali-rich compositions. Nevertheless, the analyses provide consistent geochemical trends.

Lower Sheepbed and Gillespie Lake bulk rock compositions (Fig. 2, A and B) are very tightly grouped, and slightly more mafic than average Martian crust (closer to FM apex). Most upper Sheepbed samples plot in a similar position but several trend toward the CN and CNK apexes, where Ca-sulfate plots. ChemCam analyses (Fig. 2, C and D) show a more complete linear trend, with one end member defined by Ca-sulfates within the light-toned fractures and filled hollow nodules that were targeted for analysis. The Glenelg member has bulk compositions that commonly differ from both average crust and Sheepbed/Gillespie Lake, with less relative amounts of $FeO_T$+MgO and higher $K_2O$ in some samples, characteristics confirmed by ChemCam analyses that also show evidence for detrital feldspar (Fig. 2D). An analysis of APXS data for the Yellowknife Bay formation samples Bathurst Inlet and Rocknest3, as well as the float rocks Jake_Matijevic (Jake_M) and Et Then on Bradbury Rise, which have been inferred to be volcaniclastic or igneous, shows that the elemental relationships among these rocks are consistent with physical mixing between Bathurst Inlet-like and Jake_M-like material with addition of an Fe-rich cement or rind, especially apparent in Et_Then (*28*). Some ChemCam analyses plot above the plagioclase–K-feldspar and feldspar-FM joins suggesting phyllosilicate-rich targets, consistent with the identification of phyllosilicates by XRD (*4*). In addition, some ChemCam Sheepbed analyses plot closer to the FM apex, consistent with the identification of Mg-Fe-Cl-rich phases associated with raised ridges (also observed in the McGrath APXS raster) that were also targeted for analysis (see below) and the $Fe^{3+}$-rich phases identified by XRD (e.g., magnetite, akaganeite, and possibly hematite).

Despite identifying phyllosilicates in Sheepbed mudstones by XRD (*4*) and inferring them from ChemCam (Fig. 2, C and D), the geochemistry of the Yellowknife Bay formation provides scant support for any substantial chemical weathering history affecting the sources or the sediment during transport into the depositional basin. During circum-neutral pH weathering, clay minerals form at the expense of primary igneous phases, with loss of mobile elements. As a result, bulk sedimentary rock compositions that have been influenced by weathering, including those derived from mafic sources, typically plot above the plagioclase–K-feldspar and feldspar-FM joins (*29*–*31*). Similarly, any clay minerals that formed by hydrothermal alteration (e.g., impact-related) in surrounding regions and transported into the Yellowknife basin would also carry comparable distinct chemical signatures (*22*, *32*–*34*). Nor is any evidence observed for low pH alteration conditions, in the form of $Fe^{3+}$ mobility and associated formation of $Fe^{3+}$-sulfates, such as that observed by the Spirit and Opportunity rovers (*35*–*37*). During transport, clays concentrate in fine-grained sediment (i.e., Sheepbed) compared to associated coarse-grained sediment (i.e., Gillespie Lake) but no evidence for the predicted geochemical fractionation related to hydraulic segregation of sediment types (including clay minerals and magnetite) is observed in the bulk analyses of either unit.

One complicating factor is that secondary Ca-sulfate might lower apparent CIA values and mask evidence for chemical weathering (*27*). However, on a plot of CIA versus $SO_3$ content (Fig. 3), this clearly is not the case. At high $SO_3$, indicative of sulfates, CIA falls to lower values as expected but at lower $SO_3$, CIA levels off to values typical of Martian mafic igneous rocks thus indicating that none of these samples has witnessed a substantial chemical weathering history. This is also consistent with sample positions on the A-CNK-FM diagram (Fig. 2B). Accordingly, formation of phyllosilicates within Sheepbed mudstones likely resulted from diagenetic processes that did not noticeably influence bulk rock composition, implying rock-dominated (i.e., low water/rock ratio) post-depositional aqueous fluid conditions.

Both major and trace elements exhibit stratigraphic trends (Fig. 4). To avoid variations in absolute abundances imparted by simple dilution effects of Ca-sulfate, we plot ratios among elements most often associated with siliciclastic components. On a plot of $K_2O/Al_2O_3$ versus $TiO_2/Al_2O_3$ (Fig. 4A) the Glenelg member includes samples with higher $K_2O/Al_2O_3$ and generally have slightly more variable $TiO_2/Al_2O_3$, compared to the Sheepbed and Gillespie Lake members. The two analyses from the rock Bathurst Inlet, from the top of the Glenelg member, are especially distinctive in having the highest $K_2O/Al_2O_3$ ratios. These differences are interpreted to represent a notable change in the provenance from which sediment particles were derived to include more alkali-rich basalts higher in the stratigraphic section.

Subtle differences in bulk composition also exist within the Sheepbed member itself, with the upper part of the member having slightly lower and more variable $TiO_2/Al_2O_3$ ($x$ = 0.104, SD = 0.011) than the lower part ($x$ = 0.116, SD = 0.006). This could also be a subtle provenance effect (*38*, *39*), although relationships between $TiO_2/Al_2O_3$ ratio and overall bulk composition is complex in detail, especially because all compositions are basaltic (*12*, *40*). In addition, small variations in plagioclase content that are ultimately related to sedimentary sorting effects (*24*), could also play a role in changing the $TiO_2/Al_2O_3$ ratio (Fig. 4A).

Stratigraphic variations in APXS trace elements are summarized on a plot of Cr/Ni versus Zn/Ni (Fig. 4B). In this case, the Glenelg member has higher and/or more variable ratios than the Sheepbed member, related to combinations of elevated Zn and Cr and lower Ni. There is also a difference between the Gillespie Lake sandstone and Sheepbed mudstones, related mainly to lower Ni in the former, although only a single high quality analysis is available for the Gillespie Lake member. Major elements indicate a similar provenance and so the reason for this is not clear. A heavy mineral effect is one possibility but would be more likely to cause an enrichment of Cr (chromite) rather than depletion of Ni in the sandstones. Thus, in Glenelg sandstones, Ni is similarly low (~200-400 ppm) as in the Gillespie Lake sandstone sample but Cr reaches very high levels (>5000 ppm) consistent with a heavy mineral (chromite) enrichment predicted by fluvial processing (*41*). Within the Sheepbed member, the upper part has lower Cr/Ni and Zn/Ni, related mainly to higher Ni, consistent with a slightly different, but still mafic, provenance.

Lithium contents measured by ChemCam (*42*) also reveal a stratigraphic trend (Fig. 4C) with Sheepbed mudstones having low and uniform abundances ($x$ = 4.3 ppm; SD = 2.4 ppm) whereas the overlying units have about a factor of two higher and much more variable Li abundances. Although secondary aqueous processes, such as hydrothermal activity, can enrich Li (*43*) and evidence for centimeter-scale Li redistribution is observed in diagenetic raised ridges (see below), this range for average values probably cannot be distinguished from variations in basaltic provenance given our limited understanding of Li distributions in the Martian crust-mantle system.

**Early Diagenetic Features**

Efforts were made to characterize chemical and mineralogical controls on concretion formation within the Sheepbed member. Numerous ChemCam observations were directed at concretions but no systematic differences were observed, limiting compositional differences between

concretion and host sediment to less than ~10% for major elements. APXS analyses of drill fines from concretion+hollow nodule-rich (Cumberland) and concretion+hollow nodule-poor (John_Klein) areas were also examined (*25*) (table S5). Samples delivered to the internal instruments (CheMin and SAM) that determined mineralogy (*3*, *4*) are preferable and can be analyzed by APXS after being dumped onto the surface when CheMin and SAM analyses are complete (as for John_Klein). However, at the time of writing, Curiosity was still carrying the Cumberland sample and consequently it has not been analyzed by APXS and instead analysis of the fines that accumulated around the drill hole from the drilling process were used. Additionally, imaging of drill hole walls indicates John_Klein has greater amounts of Ca-sulfate-filled fractures (see below). A two-stage calculation was thus performed to evaluate results. First, 5% anhydrite was removed from the John_Klein composition to put $SO_3$ at similar concentrations in both samples, and broadly consistent with mapping veins in drill hole walls (*4*). Second, two gain-loss calculations were performed assuming Ti and Al, respectively, are constant between samples. Elements enriched (taken as ≥5% in both calculations) in Cumberland include Fe, Ca, Cl, Br, Ni, and Ge. Elevated Ca is difficult to interpret given the Ca-sulfate in fractures but elevated Fe, Cl, Br and Ni are consistent with small amounts of a minor mineral such as akaganeite, identified by XRD, forming at least part of the concretion cement (*4*).

ChemCam and APXS analyses of isopachous cements within early diagenetic raised ridges indicate the presence of a Mg-Fe-Cl rich phase (or assemblage). ChemCam confirms that the amount of MgO is as high as ~17%, and in places is accompanied by elevated Li (Fig. 5A). The observation that Li and Mg are not well correlated across the different layers of isopachous cements (e.g., right hand side of Fig. 5A image) suggests a complex origin. APXS rasters on the raised ridge target McGrath further indicates elevated Fe and that both Mg and Fe correlate with Cl, although enrichment of any chloride phase or oxychlorine compound explains only a tiny part of the Mg-Fe variation (Fig. 5B). A mass balance calculation using the highest and lowest APXS MgO analyses from the McGrath raster (McGrath-R1 and -R2) and assuming the component is ~20% of the rock indicates a composition of $SiO_2$ ~ 45%; $FeO_T$ ~ 35%; MgO ~ 18%, Cl ~ 3% and ~1300-1500 ppm each for Ni, Zn and Br (*25*) (table S6). Such a composition cannot be accommodated by any single phase identified in the drilled samples by XRD, but perhaps is consistent with a mixture of Mg-rich, Al-deficient smectitic clay (e.g., hectorite, stevensite) and halogen-bearing Fe-oxides (e.g., akaganeite).

**Late Diagenetic Features**

Both ChemCam and APXS provide constraints on the mineralogy of cross-cutting late diagenetic light-toned fractures, including filled hollow nodules. ChemCam shots on these features (Fig. 5C) show elevated Ca, S and in places H, indicating multiple hydration states of Ca-sulfate. ChemCam also measured elevated Sr content (up to 450 ppm) in the fracture fills (Fig. 5C), as expected for Ca-sulfate (*44*). The presence of multiple Ca-sulfate minerals is also consistent with CheMin XRD analyses that identified anhydrite and bassanite (but not gypsum) and MastCam VNIR spectroscopy that suggests that some fracture fills are hydrated, possibly indicating gypsum (*4*). Finally, APXS raster analysis on the fracture fill target Sayunei also indicates the presence of Ca-sulfates through a correlation between CaO and $SO_3$, the slope of which is consistent with $CaSO_4$ stoichiometry (Fig. 5D).

The composition of the dike-like "snake" feature (Snake_River target) may bear on its origin The Snake_River major element composition is most similar to sedimentary rocks in the lower part of the Yellowknife Bay formation and best matches the lower Sheepbed member for major elements (Fig. 6A); it differs from the Gillespie Lake member for S, Cl and all trace elements (Fig. 6B). Although close similarity exists with individual analyses of the heterogeneous Glenelg member, the "snake" does not compare favorably to the Glenelg average for a number of elements (Fig. 6C) suggesting it probably did not result from infall of overlying sediment into a fracture. These comparisons indicate that the composition of the snake is consistent with a sedimentary dike, as suggested from stratigraphic relationships (*2*), intruded from the Sheepbed or unexposed sediments at lower stratigraphic levels and not currently exposed. In detail, its trace element composition differs from all exposed units (higher Cr, lower Ni) suggesting an origin from a different, presumably lower, stratigraphic level.

**Discussion**

Elemental geochemistry reveals a fundamental provenance change during deposition of the Yellowknife Bay formation. Clastic sediments of the Sheepbed and Gillespie Lake members were derived from a source similar to the average Martian crust but slightly more mafic and Fe-rich ($SiO_2$ ~ 46% versus 49%; $FeO_T$ ~ 21.5% versus 18%), whereas high-K alkaline igneous rocks contribute substantially to the Glenelg member provenance. The change in provenance may be related to erosional evolution of drainage basins feeding the alluvial fan system. Down-cutting fluvial channels in the catchment of the fan system may have encountered a distinct alkaline basalt bedrock lithology (likely related to Jake_Matijevic-type composition) or captured a drainage underlain by such lithologies leading to the abrupt change in sediment provenance. On the other hand, alkaline basalts of the type suggested to be incorporated into Glenelg sediments are rare on Earth (*45*) and having them represent a dominant provenance component in distal facies of a fluvial system is unexpected and could suggest that such rocks, which have also been observed in Gusev Crater (*46*), are more common on Mars than previously thought (*45–47*). An alternative possibility is that an exotic source of alkaline basalts was locally introduced into the basin, by way of volcanic ash or flows, and reflecting relatively small volumes of alkaline basalt that in turn were locally recycled and preserved as volcaniclastic layers. This scenario is consistent with the observation that high-K signatures appear restricted to certain beds within the Glenelg member. Given the limited stratigraphic distribution that has been studied (Glenelg member exhibiting the high-K signature represents only ~1.7 m of a ~5 m section) it is not possible to distinguish whether relatively local or more regionally exposed high-K lithologies caused the provenance change and thus the scale of any potential alkaline igneous province is not well constrained from the sedimentary data.

Martian soils likely contain a small (~1-3%) meteoritic component (*48*) and estimates of crustal composition (notably Ni) are derived by assuming a 2% meteoritic soil component (*12*). Sheepbed mudstones, if deposited in an ancient lake that represented the terminus of a watershed, might be expected to contain meteoritic material that was swept into the basin. Provenance effects alone can explain the levels of Ni (~450-850 ppm) in the Sheepbed member given the slightly more mafic and Fe-rich composition, compared to average Martian crust. However, trace element data are also consistent with a modest meteoritic contribution. Modeling the effects of adding an average CI-type carbonaceous chondrite composition to average Martian crust and to one of the brushed lower Sheepbed analyses (Ekwir_Brush) shows that the low Cr/Ni and Zn/Ni ratios of the Sheepbed member are consistent with ~1-4% CI component, with a larger amount in the upper part of the member (Fig. 4B). For typical CI-type chondritic compositions (*49*), a 1-4% meteoritic component could also deliver as much as ~300-1200 ppm organic C, consistent with low levels of carbon detected by SAM (*3*).

In the absence of a fossil record, sediment chemistry is one of the few tools available to evaluate paleoclimate, by constraining chemical weathering intensity (*10*, *50*, *51*). Low CIA values and positions on A-CN-K and A-CNK-FM diagrams for the Yellowknife Bay formation (Fig. 2) indicate very limited chemical weathering prior to deposition. The similarity between major elements of the Gillespie Lake bedload-

dominated sandstones and Sheepbed member suspended load-dominated mudstones also suggests that the fluvial system carried a very high ratio of solid to dissolved river loads ($L_s/L_d$), which in turn results from both arid conditions and rapid erosion and transport (*51*, *52*) and could have been further enhanced by cold conditions that would kinetically inhibit chemical weathering reactions. Accordingly, Yellowknife Bay formation geochemistry is consistent with some combination of a highly arid, possibly frigid, climate and/or a high relief fluvial system, and probably both. On early Mars, impact processes may have aided in the generation of sedimentary particles, increasing the efficiency of physical denudation (*53*, *54*). Surface waters with low $L_d$ significantly contrasts with the high ionic strength ancient surface waters suggested at Meridiani Planum (*55*), even though both apparently record evidence of an arid climate system. In spite of the suggested arid conditions, relatively small amounts of chemical sedimentation (e.g., sulfates, carbonates, chlorides) may be expected in the Yellowknife Bay sedimentary system. In addition, to the degree that this surface water contributes to the regional groundwater system, it would also tend to promote dilute, circum-neutral subsurface aqueous conditions.

Elemental geochemistry also provides constraints on diagenetic history. The uniform bulk rock compositions of Sheepbed mudstones is particularly important, along with its suite of complex diagenetic features, which suggest post-depositional aqueous alteration took place at combined low water/rock ratios and pH levels modest enough that mineralogical changes took place under nearly isochemical conditions; very little mass has been removed from the system. Therefore, the broad array of secondary minerals identified by XRD, including saponitic phyllosilicates, magnetite, akaganeite, hematite and perhaps a substantial part of the amorphous component, needs to be explained by plausible reactions taking place within the sediment (*4*). One important exception is that textural and geochemical relationships indicate Ca-sulfates, found in fractures, voids and hollow nodules, were later "added" to the rock and not formed by local redistribution of elements during the earlier stage of diagenesis that transformed the Sheepbed sediment to rock. Thus, at least two distinct diagenetic fluid events took place with distinct fluid chemistry. The first fluid event (perhaps more than one event, given the mineralogical complexity, including co-existence of magnetite, akaganeite, pyrrhotite and possibly hematite and pyrite) resulted in the mineral assemblage within the host sediment (and perhaps the Fe-Mg-Cl-rich assemblage associated with early diagenetic raised ridges). Plausible reactions that could be involved include olivine (+Al) ⇒ saponite + magnetite (*4*) and pyrrhotite (+pyrite?) ⇒ akaganeite (⇒ hematite?), the latter of which would be promoted by $Cl^-$-bearing fluids that also in turn could have promoted concretion formation. Sometime after lithification, an additional fluid event, presumably originating from deeper within the section and associated with fracturing of the mudstone, injected fluids that became saturated with respect to Ca-sulfate (typically early precipitated minerals in evolving brines) due to changing chemistry and/or pressure-temperature conditions. These fluids precipitated sulfates within the fractures, and filled any void spaces that the fractures intersected, including the hollow nodules. Although considerable modeling and experimental effort will be required to fully understand these processes, it is possible to construct simple forward thermochemical aqueous models broadly consistent with these observations (*25*) (fig. S8).

Our findings add to the growing evidence for highly diverse sedimentary environments on early Mars (*2*, *56*, *57*). The Burns formation of Meridiani Planum is the only sedimentary sequence that has been studied in situ in comparable detail and is of similar age—if anything, even older (*20*, *57*, *58*). Although both represent clastic sedimentation derived from basalt sources and influenced by complex groundwater diagenesis, the sedimentary history is strikingly different. For example, where the Burns formation preserves evidence for very low pH and very high ionic strength groundwater, the Yellowknife Bay formation had relatively dilute circum-neutral groundwater. Where the Burns formation is dominated by chemically precipitated constituents (sulfates, chlorides) derived from evaporation of acidic brines, Yellowknife Bay mudstones contain very little in the way of chemically precipitated constituents and, apart from cross-cutting Ca-sulfate veins, the secondary mineralogy formed mostly within a largely closed geochemical system. Where the basaltic debris within the Burns was substantially chemically weathered prior to deposition, Yellowknife Bay detritus appears to be essentially unweathered. Orbital spectroscopic mapping suggests that surface aqueous environmental conditions on early Mars (late Noachian) evolved from circum-neutral clay-rich to acidic sulfate-rich settings (*59*), but it would appear, just like on Earth where evolving global environments are also reflected in the broad sweep of the sedimentary record (*60*), that when faced with rocks on the ground, geological complexity is apparently inevitable.

**Materials and Methods**

APXS is a well-established analytical technique on Mars, providing quantitative abundance data for major and minor elements, including S and Cl, and trace elements Cr, Ni, Zn, Ge and Br (*61*). Analytical details are provided in the supplementary materials (*25*) and Yellowknife Bay formation results are provided in tables S1 to S4. Multiple APXS analyses were sometimes obtained on the same rock but at different locations. In some cases (e.g., Bathurst Inlet) both analyses are considered because they represent slightly different stratigraphic levels. However, where multiple analyses were made at a single site, such as drill sites (e.g., John_Klein, Cumberland) and APXS "rasters" (e.g., Sayunei, McGrath), the analysis with lowest $SO_3$ was selected as most representative of the sedimentary rock because brushed surfaces indicate low $SO_3$ and mapping of borehole walls suggests Ca-sulfate abundances correlate with diagenetic light-toned veins and hollow nodule fills. APXS "rasters," involving multiple, closely spaced measurements, were employed on two diagenetic features: fracture fills (Sayunei) and raised ridges (McGrath) and these results are provided in table S4, which also includes the suggested sedimentary dike (Snake_River analysis). The ChemCam LIBS instrument provides semiquantitative analyses for major and some minor and trace elements (e.g., Ba, Rb, Sr, Li) using multiple laser pulses (shots) on ~350-550 μm diameter targets from up to 7 m distance (*62*, *63*). The first ~5 shots remove surface dust and the rock analyses are based on averages of subsequent shots. Further analytical details are provided in the supplemental information (*25*).

**References and Notes**


1. Names have been assigned to certain areographic features by the Mars Science Laboratory (MSL) team for planning and operations purposes. The names are not formally recognized by the International Astronomical Union.
2. J. P. Grotzinger, D. Y. Sumner, L. C. Kah, K. Stack, S. Gupta, L. Edgar, D. Rubin, K. Lewis, J. Schieber, N. Mangold, R. Milliken, P. G. Conrad, D. DesMarais, J. Farmer, K. Siebach, F. Calef, III, J. Hurowitz, S. M. McLennan, D. Ming, D. Vaniman, J. Crisp, A. Vasavada, K. S. Edgett, M. Malin, D. Blake, R. Gellert, P. Mahaffy, R. C. Wiens, S. Maurice, J. A. Grant, S. Wilson, R. C. Anderson, L. Beegle, R. Arvidson, B. Hallet, R. S. Sletten, M. Rice, J. Bell, III, J. Griffes, B. Ehlmann, R. B. Anderson, T. F. Bristow, W. E. Dietrich, G. Dromart, J. Eigenbrode, A. Fraeman, C. Hardgrove, K. Herkenhoff, L. Jandura, G. Kocurek, S. Lee, L. A. Leshin, R. Leveille, D. Limonadi, J. Maki, S. McCloskey, M. Meyer, M. Minitti, H. Newsom, D. Oehler, A. Okon, M. Palucis, T. Parker, S. Rowland, M. Schmidt, S. Squyres, A. Steele, E. Stolper, R. Summons, A. Treiman, R. Williams, A. Yingst, MSL Science Team, A habitable fluvio-lacustrine environment at Yellowknife Bay, Gale Crater, Mars. *Science* **343**, 1242777 (2014); 10.1126/science.1242777.
3. D. W. Ming, P. D. Archer Jr., D. P. Glavin, J. L. Eigenbrode, H. B. Franz, B. Sutter, A. E. Brunner, J. C. Stern, C. Freissinet, A. C. McAdam, P. R. Mahaffy, M. Cabane, P. Coll, J. L. Campbell, S. K. Atreya, P. B. Niles, J. F. Bell III, D. L. Bish, W. B. Brinckerhoff, A. Buch, P. G. Conrad, D. J. Des Marais, B. L. Ehlmann, A. G. Fairén, K. Farley, G. J. Flesch, P. Francois, R.

Gellert, J. A. Grant, J. P. Grotzinger, S. Gupta, K. E. Herkenhoff, J. A. Hurowitz, L. A. Leshin, K. W. Lewis, S. M. McLennan, K. E. Miller, J. Moersch, R. V. Morris, R. Navarro-González, A. A. Pavlov, G. M. Perrett, I. Pradler, S. W. Squyres, R. E. Summons, A. Steele, E. M. Stolper, D. Y. Sumner, C. Szopa, S. Teinturier, M. G. Trainer, A. H. Treiman, D. T. Vaniman, A. R. Vasavada, C. R. Webster, J. J. Wray, R. A. Yingst, MSL Science Team, Volatile and organic compositions of sedimentary rocks at Yellowknife Bay, Gale Crater, Mars. *Science* **343**, 1245267 (2014); 10.1126/science.1245267.

4. D. T. Vaniman, D. L. Bish, D. W. Ming, T. F. Bristow, R. V. Morris, D. F. Blake, S. J. Chipera, S. M. Morrison, A. H. Treiman, E. B. Rampe, M. Rice, C. N. Achilles, J. Grotzinger, S. M. McLennan, J. Williams, J. Bell III, H. Newsom, R. T. Downs, S. Maurice, P. Sarrazin, A. S. Yen, J. M. Morookian, J. D. Farmer, K. Stack, R. E. Milliken, B. Ehlmann, D. Y. Sumner, G. Berger, J. A. Crisp, J. A. Hurowitz, R. Anderson, D. DesMarais, E. M. Stolper, K. S. Edgett, S. Gupta, N. Spanovich, MSL Science Team, Mineralogy of a mudstone at Yellowknife Bay, Gale Crater, Mars. *Science* **343**, 1243480 (2014); 10.1126/science.1243480.
5. H. W. Nesbitt, G. M. Young, Early Proterozoic climates and plate motions inferred from major element chemistry of lutites. *Nature* **299**, 715–717 (1982). doi:10.1038/299715a0
6. H. W. Nesbitt, G. M. Young, Petrogenesis of sediments in the absence of chemical weathering: Effects of abrasion and sorting on bulk composition and mineralogy. *Sedimentology* **43**, 341–358 (1996). doi:10.1046/j.1365-3091.1996.d01-12.x
7. S. M. McLennan, S. Hemming, D. K. McDaniel, G. N. Hanson, Geochemical approaches to sedimentation, provenance, and tectonics, in *Processes Controlling the Composition of Clastic Sediments*, M. J. Johnsson, A. Basu, Eds. *Geol. Soc. Am. Spec. Paper* **284**, 21–40 (1993).
8. H. W. Nesbitt, G. M. Young, S. M. McLennan, R. R. Keays, Effects of chemical weathering and sorting on the petrogenesis of siliciclastic sediments, with implications for provenance studies. *J. Geol.* **104**, 525–542 (1996). doi:10.1086/629850
9. C. M. Fedo, G. M. Young, H. W. Nesbitt, J. M. Hanchar, Potassic and sodic metasomatism in the Southern Provenance of the Canadian Shield: Evidence from the Paleoproterozoic Serpent Formation, Huronian Supergroup, Canada. *Precambrian Res.* **84**, 17–36 (1997). doi:10.1016/S0301-9268(96)00058-7
10. H. W. Nesbitt, Petrogenesis of siliciclastic sediments and sedimentary rocks, in *Geochemistry of Sediments and Sedimentary Rocks*, D. R. Lentz, Ed., *Geol. Assoc. Canada GeoText* **4**, 39–51 (2003).
11. S. R. Taylor, S. M. McLennan, *The Continental Crust: Its Composition and Evolution* (Blackwells, Oxford, 1985).
12. S. R. Taylor, S. M. McLennan, *Planetary Crusts: Their Composition, Origin and Evolution* (Cambridge Univ. Press, Cambridge, 2009).
13. G. M. Young, H. W. Nesbitt, Paleoclimatology and provenance of the glaciogenic Gowganda Formation (Paleoproterozoic), Ontario, Canada: A chemostratigraphic approach. *Geol. Soc. Am. Bull.* **111**, 264–274 (1999). doi:10.1130/0016-7606(1999)111<0264:PAPOTG>2.3.CO;2s
14. P. Michalopoulos, R. C. Aller, Rapid clay mineral formation in Amazon Delta sediments: Reverse weathering and oceanic elemental cycles. *Science* **270**, 614–617 (1995). doi:10.1126/science.270.5236.614
15. M. A. Chan, J. Ormö, A. J. Park, M. Stich, V. Souza-Egipsy, G. Komatsu, Models of iron oxide concretion formation: Field, numerical, and laboratory comparisons. *Geofluids* **7**, 356–368 (2007). doi:10.1111/j.1468-8123.2007.00187.x
16. B. C. Clark, R. V. Morris, S. M. McLennan, R. Gellert, B. Jolliff, A. H. Knoll, S. W. Squyres, T. K. Lowenstein, D. W. Ming, N. J. Tosca, A. Yen, P. R. Christensen, S. Gorevan, J. Brückner, W. Calvin, G. Dreibus, W. Farrand, G. Klingelhoefer, H. Waenke, J. Zipfel, J. F. Bell, III, J. Grotzinger, H. Y. McSween, R. Rieder, Chemistry and mineralogy of outcrops at Meridiani Planum. *Earth Planet. Sci. Lett.* **240**, 73–94 (2005). doi:10.1016/j.epsl.2005.09.040
17. S. M. McLennan, J. F. Bell, III, W. M. Calvin, P. R. Christensen, B. C. Clark, P. A. de Souza, J. Farmer, W. H. Farrand, D. A. Fike, R. Gellert, A. Ghosh, T. D. Glotch, J. P. Grotzinger, B. Hahn, K. E. Herkenhoff, J. A. Hurowitz, J. R. Johnson, S. S. Johnson, B. Jolliff, G. Klingelhöfer, A. H. Knoll, Z. Learner, M. C. Malin, H. Y. McSween, Jr., J. Pocock, S. W. Ruff, L. A. Soderblom, S. W. Squyres, N. J. Tosca, W. A. Watters, M. B. Wyatt, A. Yen, Provenance and diagenesis of the evaporite-bearing Burns formation, Meridiani Planum, Mars. *Earth Planet. Sci. Lett.* **240**, 95–121 (2005). doi:10.1016/j.epsl.2005.09.041
18. J. A. Hurowitz, S. M. McLennan, H. Y. McSween, Jr., P. A. DeSouza, Jr., G. Klingelhöfer, Mixing relationships and the effects of secondary alteration in the Wishstone and Watchtower classes of Husband Hill, Gusev Crater, Mars. *J. Geophys. Res. Planets* **111**, (E12), E12S14 (2006). doi:10.1029/2006JE002795
19. A. H. Knoll, B. L. Jolliff, W. H. Farrand, J. F. Bell, III, B. C. Clark, R. Gellert, M. P. Golombek, J. P. Grotzinger, K. E. Herkenhoff, J. R. Johnson, S. M. McLennan, R. Morris, S. W. Squyres, R. Sullivan, N. J. Tosca, A. Yen, Z. Learner, Veneers, rinds, and fracture fills: Relatively late alteration of sedimentary rocks at Meridiani Planum, Mars. *J. Geophys. Res. Planets* **113**, E06S16 (2008). doi:10.1029/2007JE002949
20. S. M. McLennan, J. P. Grotzinger, The sedimentary rock cycle of Mars, in *The Mars Surface: Composition, Mineralogy and Physical Properties*, J. F. Bell III, Ed. (Cambridge Univ. Press, Cambridge, 2008), pp. 541–577.
21. S. W. Squyres, R. E. Arvidson, J. F. Bell, 3rd, F. Calef, 3rd, B. C. Clark, B. A. Cohen, L. A. Crumpler, P. A. de Souza, Jr., W. H. Farrand, R. Gellert, J. Grant, K. E. Herkenhoff, J. A. Hurowitz, J. R. Johnson, B. L. Jolliff, A. H. Knoll, R. Li, S. M. McLennan, D. W. Ming, D. W. Mittlefehldt, T. J. Parker, G. Paulsen, M. S. Rice, S. W. Ruff, C. Schröder, A. S. Yen, K. Zacny, Ancient impact and aqueous processes at Endeavour Crater, Mars. *Science* **336**, 570–576 (2012). doi:10.1126/science.1220476 Medline
22. B. L. Ehlmann, J. F. Mustard, S. L. Murchie, J. P. Bibring, A. Meunier, A. A. Fraeman, Y. Langevin, Subsurface water and clay mineral formation during the early history of Mars. *Nature* **479**, 53–60 (2011). doi:10.1038/nature10582 Medline
23. A. Wang, R. L. Korotev, B. L. Jolliff, L. A. Haskin, L. Crumpler, W. H. Farrand, K. E. Herkenhoff, P. de Souza Jr., A. G. Kusack, J. A. Hurowitz, N. J. Tosca, Evidence of phyllosilicates in Wooly Patch, an altered rock encountered at West Spur, Columbia Hills, by the Spirit rover in Gusev Crater, Mars. *J. Geophys. Res. Planets* **111**, E02S16 (2006). doi:10.1029/2005JE002516
24. I. O. McGlynn, C. M. Fedo, H. Y. McSween, Jr., Soil mineralogy at the Mars Exploration Rover landing sites: An assessment of the competing roles of physical sorting and chemical weathering. *J. Geophys. Res. Planets* **117**, (E1), E01006 (2012). doi:10.1029/2011JE003861
25. Supplementary materials are available on *Science* Online.
26. A. S. Yen, R. Gellert, C. Schröder, R. V. Morris, J. F. Bell, 3rd, A. T. Knudson, B. C. Clark, D. W. Ming, J. A. Crisp, R. E. Arvidson, D. Blaney, J. Brückner, P. R. Christensen, D. J. DesMarais, P. A. de Souza, Jr., T. E. Economou, A. Ghosh, B. C. Hahn, K. E. Herkenhoff, L. A. Haskin, J. A. Hurowitz, B. L. Joliff, J. R. Johnson, G. Klingelhöfer, M. B. Madsen, S. M. McLennan, H. Y. McSween, L. Richter, R. Rieder, D. Rodionov, L. Soderblom, S. W. Squyres, N. J. Tosca, A. Wang, M. Wyatt, J. Zipfel, An integrated view of the chemistry and mineralogy of martian soils. *Nature* **436**, 49–54 (2005). doi:10.1038/nature03637 Medline
27. In order to focus on relationships among silicate mineralogy, A-CN-K and A-CNK-FM diagrams normally correct CaO for the presence of carbonates and sedimentary Ca-phosphates (CaO*) and in rare cases correct $Na_2O$ for the presence of halite ($Na_2O$*). In Martian settings, attempts at making corrections for chemical constituents have commonly proven nonunique because mineralogical determinations are either incomplete or do not exist and nonsilicate mineralogy is both uncertain and complex, involving a variety of Ca-, Mg-, and Fe-sulfates, chlorides, perchlorates, and in some cases carbonates. Accordingly, bulk analyses are used in formulating these diagrams and the CIA values and the possibility of nonsilicate phases must be considered when making interpretations.
28. M. E. Schmidt *et al*., APXS of first rocks encountered by Curiosity in Gale Crater: Geochemical diversity and volatile element (K and Zn) enrichment. *Lunar Planet. Sci. Conf.* **44**, Abstract 1278 (2013).
29. K. Stamatelopoulou-Seymour, D. M. Francis, An Archean ultramafic turbidite from Lac Guyer, James Bay area, Quebec, Canada. *Can. J. Earth Sci.* **17**, 1576–1582 (1980). doi:10.1139/e80-164
30. H. W. Nesbitt, G. M. Young, S. A. Bosman, Major and trace element geochemistry and genesis of supracrustal rocks of the North Spirit Lake greenstone belt, NW Ontario, Canada. *Precambrian Res.* **174**, 16–34 (2009). doi:10.1016/j.precamres.2009.06.006
31. S. Saha, S. Banerjee, S. D. Burley, A. Ghosh, P. K. Saraswati, The influence

of flood basaltic source terrains on the efficiency of tectonic setting discrimination diagrams: An example from the Gulf of Khambhat, western Inda. *Sediment. Geol.* **228**, 1–13 (2010). doi:10.1016/j.sedgeo.2010.03.009

32. L. L. Griffith, E. L. Shock, Hydrothermal hydration of Martian crust: illustration via geochemical model calculations. *J. Geophys. Res. Planets* **102**, 9135–9143 (1997). doi:10.1029/96JE02939 Medline
33. J. A. Hurowitz , S. M. McLennan, D. H. Lindsley, M. A. A. Schoonen, Experimental epithermal alteration of synthetic Los Angeles meteorite: Implications for the origin of Martian soils and identification of hydrothermal sites on Mars. *J. Geophys. Res. Planets* **110**, E07002 (2005). doi:10.1029/2004JE002391
34. M. V. Naumov, Principal features of impact-generated hydrothermal circulation systems: Mineralogical and geochemical evidence. *Geofluids* **5**, 165–184 (2005). doi:10.1111/j.1468-8123.2005.00092.x
35. N. J. Tosca, S. M. McLennan, B. C. Clark, J. P. Grotzinger, J. A. Hurowitz, A. H. Knoll, C. Schröder, S. W. Squyres, Geochemical modeling of evaporation processes on Mars: Insight from the sedimentary record at Meridiani Planum. *Earth Planet. Sci. Lett.* **240**, 122–148 (2005). doi:10.1016/j.epsl.2005.09.042
36. J. A. Hurowitz, S. M. McLennan, N. J. Tosca, R. E. Arvidson, J. R. Michalski, D. W. Ming, C. Schröder, S. W. Squyres, In situ and experimental evidence for acidic weathering on Mars. *J. Geophys. Res.* **111**, E02S19 (2006). doi:10.1029/2005JE002515
37. P. L. King, H. Y. McSween, Jr., Effects of $H_2O$, pH and oxidation state on the stability of Fe-minerals on Mars. *J. Geophys. Res. Planets* **110**, (E12), E12S10 (2005). doi:10.1029/2005JE002482
38. G. M. Young, H. W. Nesbitt, Processes controlling the distribution of Ti and Al in weathering profiles, siliciclastic sediments and sedimentary rocks. *J. Sed. Res.* **68**, 448–455 (1998). doi:10.2110/jsr.68.448
39. N. C. Martinez, R. W. Murray, R. C. Thunell, L. C. Peterson, F. Muller-Karger, L. Lorenzoni, Y. Astor, R. Varela, Local and regional geochemical signatures of surface sediments from the Cariaco Basin and Orinoco Delta, Venezuela. *Geology* **38**, 159–162 (2010). doi:10.1130/G30487.1
40. Basaltic Volcanism Study Project, *Basaltic Volcanism on the Terrestrial Planets* (Pergamon, New York, 1981).
41. R. Slingerland, N. D. Smith, Occurrence and formation of waterlaid placers. *Annu. Rev. Earth Planet. Sci.* **14**, 113–147 (1986). doi:10.1146/annurev.ea.14.050186.000553
42. A. M. Ollila *et al*., Early results from Gale Crater on ChemCam detections of carbon, lithium, and rubidium. *Lunar Planet. Sci. Conf.* **44**, Abstract 2188 (2013).
43. L.-H. Chan, J. C. Alt, D. A. H. Teagle, Lithium and lithium isotope profiles through the upper oceanic crust: A study of seawater-basalt exchange at ODP Sites 504A and 896A. *Earth Planet. Sci. Lett.* **201**, 187–201 (2002). doi:10.1016/S0012-821X(02)00707-0
44. F. H. Lu, W. J. Meyers, G. N. Hanson, Trace elements and environmental significance of Messinian gypsum deposits, the Nijar Basin, southeastern Spain. *Chem. Geol.* **192**, 149–161 (2002). doi:10.1016/S0009-2541(02)00009-8
45. E. M. Stolper, M. B. Baker, M. E. Newcombe, M. E. Schmidt, A. H. Treiman, A. Cousin, M. D. Dyar, M. R. Fisk, R. Gellert, P. L. King, L. Leshin, S. Maurice, S. M. McLennan, M. E. Minitti, G. Perrett, S. Rowland, V. Sautter, R. C. Wiens, O. Kemppinen, N. Bridges, J. R. Johnson, D. Cremers, J. F. Bell, L. Edgar, J. Farmer, A. Godber, M. Wadhwa, D. Wellington, I. McEwan, C. Newman, M. Richardson, A. Charpentier, L. Peret, J. Blank, G. Weigle, S. Li, R. Milliken, K. Robertson, V. Sun, C. Edwards, B. Ehlmann, K. Farley, J. Griffes, J. Grotzinger, H. Miller, C. Pilorget, M. Rice, K. Siebach, K. Stack, C. Brunet, V. Hipkin, R. Leveille, G. Marchand, P. S. Sanchez, L. Favot, G. Cody, A. Steele, L. Fluckiger, D. Lees, A. Nefian, M. Martin, M. Gailhanou, F. Westall, G. Israel, C. Agard, J. Baroukh, C. Donny, A. Gaboriaud, P. Guillemot, V. Lafaille, E. Lorigny, A. Paillet, R. Perez, M. Saccoccio, C. Yana, C. Armiens-Aparicio, J. C. Rodriguez, I. C. Blazquez, F. G. Gomez, J. Gomez-Elvira, S. Hettrich, A. L. Malvitte, M. M. Jimenez, J. Martinez-Frias, J. Martin-Soler, F. J. Martin-Torres, A. M. Jurado, L. Mora-Sotomayor, G. M. Caro, S. N. Lopez, V. Peinado-Gonzalez, J. Pla-Garcia, J. A. R. Manfredi, J. J. Romeral-Planello, S. A. S. Fuentes, E. S. Martinez, J. T. Redondo, R. Urqui-O'Callaghan, M.-P. Z. Mier, S. Chipera, J.-L. Lacour, P. Mauchien, J.-B. Sirven, H. Manning, A. Fairen, A. Hayes, J. Joseph, S. Squyres, R. Sullivan, P. Thomas, A. Dupont, A. Lundberg, N. Melikechi, A. Mezzacappa, J. DeMarines, D. Grinspoon, G. Reitz, B. Prats, E. Atlaskin, M. Genzer, A.-M. Harri, H. Haukka, H. Kahanpaa, J. Kauhanen, O. Kemppinen, M. Paton, J. Polkko, W. Schmidt, T. Siili, C. Fabre, J. Wray, M. B. Wilhelm, F. Poitrasson, K. Patel, S. Gorevan, S. Indyk, G. Paulsen, S. Gupta, D. Bish, J. Schieber, B. Gondet, Y. Langevin, C. Geffroy, D. Baratoux, G. Berger, A. Cros, C. d'Uston, O. Forni, O. Gasnault, J. Lasue, Q.-M. Lee, P.-Y. Meslin, E. Pallier, Y. Parot, P. Pinet, S. Schroder, M. Toplis, E. Lewin, W. Brunner, E. Heydari, C. Achilles, D. Oehler, B. Sutter, M. Cabane, D. Coscia, G. Israel, C. Szopa, S. Teinturier, G. Dromart, F. Robert, S. Le Mouelic, N. Mangold, M. Nachon, A. Buch, F. Stalport, P. Coll, P. Francois, F. Raulin, J. Cameron, S. Clegg, D. DeLapp, R. Dingler, R. S. Jackson, S. Johnstone, N. Lanza, C. Little, T. Nelson, R. B. Williams, L. Kirkland, B. Baker, B. Cantor, M. Caplinger, S. Davis, B. Duston, K. Edgett, D. Fay, C. Hardgrove, D. Harker, P. Herrera, E. Jensen, M. R. Kennedy, G. Krezoski, D. Krysak, L. Lipkaman, M. Malin, E. McCartney, S. McNair, B. Nixon, L. Posiolova, M. Ravine, A. Salamon, L. Saper, K. Stoiber, K. Supulver, J. Van Beek, T. Van Beek, R. Zimdar, K. L. French, K. Iagnemma, K. Miller, R. Summons, F. Goesmann, W. Goetz, S. Hviid, M. Johnson, M. Lefavor, E. Lyness, E. Breves, C. Fassett, D. F. Blake, T. Bristow, D. DesMarais, L. Edwards, R. Haberle, T. Hoehler, J. Hollingsworth, M. Kahre, L. Keely, C. McKay, M. B. Wilhelm, L. Bleacher, W. Brinckerhoff, D. Choi, P. Conrad, J. P. Dworkin, J. Eigenbrode, M. Floyd, C. Freissinet, J. Garvin, D. Glavin, D. Harpold, P. Mahaffy, D. K. Martin, A. McAdam, A. Pavlov, E. Raaen, M. D. Smith, J. Stern, F. Tan, M. Trainer, M. Meyer, A. Posner, M. Voytek, R. C. Anderson, A. Aubrey, L. W. Beegle, A. Behar, D. Blaney, D. Brinza, F. Calef, L. Christensen, J. Crisp, L. DeFlores, B. Ehlmann, J. Feldman, S. Feldman, G. Flesch, J. Hurowitz, I. Jun, D. Keymeulen, J. Maki, M. Mischna, J. M. Morookian, T. Parker, B. Pavri, M. Schoppers, A. Sengstacken, J. J. Simmonds, N. Spanovich, M. T. Juarez, A. Vasavada, C. R. Webster, A. Yen, P. D. Archer, F. Cucinotta, J. H. Jones, D. Ming, R. V. Morris, P. Niles, E. Rampe, T. Nolan, L. Radziemski, B. Barraclough, S. Bender, D. Berman, E. N. Dobrea, R. Tokar, D. Vaniman, R. M. E. Williams, A. Yingst, K. Lewis, T. Cleghorn, W. Huntress, G. Manhes, J. Hudgins, T. Olson, N. Stewart, P. Sarrazin, J. Grant, E. Vicenzi, S. A. Wilson, M. Bullock, B. Ehresmann, V. Hamilton, D. Hassler, J. Peterson, S. Rafkin, C. Zeitlin, F. Fedosov, D. Golovin, N. Karpushkina, A. Kozyrev, M. Litvak, A. Malakhov, I. Mitrofanov, M. Mokrousov, S. Nikiforov, V. Prokhorov, A. Sanin, V. Tretyakov, A. Varenikov, A. Vostrukhin, R. Kuzmin, B. Clark, M. Wolff, O. Botta, D. Drake, K. Bean, M. Lemmon, S. P. Schwenzer, R. B. Anderson, K. Herkenhoff, E. M. Lee, R. Sucharski, M. A. P. Hernandez, J. J. B. Avalos, M. Ramos, A. Jones, M.-H. Kim, C. Malespin, I. Plante, J.-P. Muller, R. Navarro-Gonzalez, R. Ewing, W. Boynton, R. Downs, M. Fitzgibbon, K. Harshman, S. Morrison, W. Dietrich, O. Kortmann, M. Palucis, D. Y. Sumner, A. Williams, G. Lugmair, M. A. Wilson, D. Rubin, B. Jakosky, T. Balic-Zunic, J. Frydenvang, J. K. Jensen, K. Kinch, A. Koefoed, M. B. Madsen, S. L. S. Stipp, N. Boyd, J. L. Campbell, I. Pradler, S. VanBommel, S. Jacob, T. Owen, E. Atlaskin, H. Savijarvi, E. Boehm, S. Bottcher, S. Burmeister, J. Guo, J. Kohler, C. M. Garcia, R. Mueller-Mellin, R. Wimmer-Schweingruber, J. C. Bridges, T. McConnochie, M. Benna, H. Franz, H. Bower, A. Brunner, H. Blau, T. Boucher, M. Carmosino, S. Atreya, H. Elliott, D. Halleaux, N. Renno, M. Wong, R. Pepin, B. Elliott, J. Spray, L. Thompson, S. Gordon, H. Newsom, A. Ollila, J. Williams, P. Vasconcelos, J. Bentz, K. Nealson, R. Popa, L. C. Kah, J. Moersch, C. Tate, M. Day, G. Kocurek, B. Hallet, R. Sletten, R. Francis, E. McCullough, E. Cloutis, I. L. ten Kate, R. Kuzmin, R. Arvidson, A. Fraeman, D. Scholes, S. Slavney, T. Stein, J. Ward, J. Berger, J. E. Moores; MSL Science Team, The petrochemistry of Jake_M: A martian mugearite. *Science* **341**, 1239463 (2013). doi:10.1126/science.1239463 Medline
46. H. Y. McSween, S. W. Ruff, R. V. Morris, J. F. Bell, III, K. Herkenhoff, R. Gellert, K. R. Stockstill, L. L. Tornabene, S. W. Squyres, J. A. Crisp, P. R. Christensen, T. J. McCoy, D. W. Mittlefehldt, M. Schmidt, Alkaline volcanic rocks from the Columbia Hills, Gusev Crater, Mars. *J. Geophys. Res. Planets* **111**, E09S91 (2006). doi:10.1029/2006JE002698
47. H. Nekvasil, F. M. McCUBBIN, A. Harrington, S. Elardo, D. H. Lindsley, Linking the Chassigny meteorite and the Martian surface rock Backstay: Insights into igneous crustal differentiation processes on Mars. *Meteorit. Planet. Sci.* **44**, 853–869 (2009). doi:10.1111/j.1945-5100.2009.tb00773.x
48. A. S. Yen, D. W. Mittlefehldt, S. M. McLennan, R. Gellert, J. F. Bell, III, H. Y. McSween, Jr., D. W. Ming, T. J. McCoy, R. V. Morris, M. Golombek, T. Economou, M. B. Madsen, T. Wdowiak, B. C. Clark, B. L. Jolliff, C. Schröder, J. Brückner, J. Zipfel, S. W. Squyres, Nickel on Mars: Constraints

on meteoritic material at the surface. *J. Geophys. Res. Planets* **111**, E12S11 (2006). doi:10.1029/2006JE002797
49. R. Hutchison, *Meteorites: A Petrologic, Chemical and Isotopic Synthesis* (Cambridge Univ. Press, Cambridge, 2004).
50. L. J. Suttner, P. K. Dutta, Alluvial sandstone composition and paleoclimate: I. Framework mineralogy. *J. Sed. Petrol.* **56**, 329–345 (1986).
51. A. D. Stewart, The ratio of mechanical to chemical denudation in alluvial systems, derived from geochemical mass balance. *Trans. R. Soc. Edinb. Earth Sci.* **84**, 73–78 (1993). doi:10.1017/S0263593300005939
52. J.-M. Martin, M. Meybeck, Elemental mass-balance of material carried by major world rivers. *Mar. Chem.* **7**, 173–206 (1979). doi:10.1016/0304-4203(79)90039-2
53. I. O. McGlynn, C. M. Fedo, H. Y. McSween, Jr., Origin of basaltic soils at Gusev Crater, Mars, by aeolian modification of impact-generated sediment. *J. Geophys. Res. Planets* **116**, E00F22 (2011). doi:10.1029/2010JE003712
54. H. J. Melosh, *Planetary Surface Processes* (Cambridge Univ. Press, Cambridge, 2011).
55. N. J. Tosca, S. M. McLennan, M. P. Lamb, J. P. Grotzinger, Physicochemical properties of concentrated Martian surface waters. *J. Geophys. Res. Planets* **116**, E05004 (2011). doi:10.1029/2010JE003700
56. S. L. Murchie, J. F. Mustard, B. L. Ehlmann, R. E. Milliken, J. L. Bishop, N. K. McKeown, E. Z. Noe Dobrea, F. P. Seelos, D. L. Buczkowski, S. M. Wiseman, R. E. Arvidson, J. J. Wray, G. Swayze, R. N. Clark, D. J. Des Marais, A. S. McEwen, J.-P. Bibring, A synthesis of Martian aqueous mineralogy after 1 Mars year of observations from the Mars Reconnaissance Orbiter. *J. Geophys. Res. Planets* **114**, E00D06 (2009). doi:10.1029/2009JE003342
57. J. P. Grotzinger, R. E. Milliken, Eds., *Sedimentary Geology of Mars. SEPM Spec. Publ. 12* (Society for Sedimentary Geology, Tulsa, 2012).
58. S. W. Squyres, A. H. Knoll, Eds., *Sedimentary Geology at Meridiani Planum, Mars* (Elsevier, Amsterdam, 2005)
59. J.-P. Bibring, Y. Langevin, J. F. Mustard, F. Poulet, R. Arvidson, A. Gendrin, B. Gondet, N. Mangold, P. Pinet, F. Forget, M. Berthé, J. P. Bibring, A. Gendrin, C. Gomez, B. Gondet, D. Jouglet, F. Poulet, A. Soufflot, M. Vincendon, M. Combes, P. Drossart, T. Encrenaz, T. Fouchet, R. Merchiorri, G. Belluci, F. Altieri, V. Formisano, F. Capaccioni, P. Cerroni, A. Coradini, S. Fonti, O. Korablev, V. Kottsov, N. Ignatiev, V. Moroz, D. Titov, L. Zasova, D. Loiseau, N. Mangold, P. Pinet, S. Douté, B. Schmitt, C. Sotin, E. Hauber, H. Hoffmann, R. Jaumann, U. Keller, R. Arvidson, J. F. Mustard, T. Duxbury, F. Forget, G. Neukum, Global mineralogical and aqueous mars history derived from OMEGA/Mars Express data. *Science* **312**, 400–404 (2006). doi:10.1126/science.1122659 Medline
60. R. M. Hazen, D. Papineau, W. Bleeker, R. T. Downs, J. M. Ferry, T. J. McCoy, D. A. Sverjensky, H. Yang, Mineral evolution. *Am. Mineral.* **93**, 1693–1720 (2008). doi:10.2138/am.2008.2955
61. R. Gellert *et al*., Initial MSL APXS activities and observations at Gale Crater, Mars. *Lunar Planet. Sci. Conf.* **44**, Abstract 1432 (2013).
62. S. Maurice, R. C. Wiens, M. Saccoccio, B. Barraclough, O. Gasnault, O. Forni, N. Mangold, D. Baratoux, S. Bender, G. Berger, J. Bernardin, M. Berthé, N. Bridges, D. Blaney, M. Bouyé, P. Caïs, B. Clark, S. Clegg, A. Cousin, D. Cremers, A. Cros, L. DeFlores, C. Derycke, B. Dingler, G. Dromart, B. Dubois, M. Dupieux, E. Durand, L. d'Uston, C. Fabre, B. Faure, A. Gaboriaud, T. Gharsa, K. Herkenhoff, E. Kan, L. Kirkland, D. Kouach, J.-L. Lacour, Y. Langevin, J. Lasue, S. Mouélic, M. Lescure, E. Lewin, D. Limonadi, G. Manhès, P. Mauchien, C. McKay, P.-Y. Meslin, Y. Michel, E. Miller, H. E. Newsom, G. Orttner, A. Paillet, L. Parès, Y. Parot, R. Pérez, P. Pinet, F. Poitrasson, B. Quertier, B. Sallé, C. Sotin, V. Sautter, H. Séran, J. J. Simmonds, J.-B. Sirven, R. Stiglich, N. Striebig, J.-J. Thocaven, M. J. Toplis, D. Vaniman, The ChemCam instrument suite on the Mars Science Laboratory (MSL) rover: Science objectives and mast unit description. *Space Sci. Rev.* **170**, 95–166 (2012). doi:10.1007/s11214-012-9912-2
63. R. C. Wiens, S. Maurice, B. Barraclough, M. Saccoccio, W. C. Barkley, J. F. Bell, S. Bender, J. Bernardin, D. Blaney, J. Blank, M. Bouyé, N. Bridges, N. Bultman, P. Caïs, R. C. Clanton, B. Clark, S. Clegg, A. Cousin, D. Cremers, A. Cros, L. DeFlores, D. Delapp, R. Dingler, C. D'Uston, M. Darby Dyar, T. Elliott, D. Enemark, C. Fabre, M. Flores, O. Forni, O. Gasnault, T. Hale, C. Hays, K. Herkenhoff, E. Kan, L. Kirkland, D. Kouach, D. Landis, Y. Langevin, N. Lanza, F. LaRocca, J. Lasue, J. Latino, D. Limonadi, C. Lindensmith, C. Little, N. Mangold, G. Manhes, P. Mauchien, C. McKay, E. Miller, J. Mooney, R. V. Morris, L. Morrison, T. Nelson, H. Newsom, A. Ollila, M. Ott, L. Pares, R. Perez, F. Poitrasson, C. Provost, J. W. Reiter, T. Roberts, F. Romero, V. Sautter, S. Salazar, J. J. Simmonds, R. Stiglich, S. Storms, N. Striebig, J.-J. Thocaven, T. Trujillo, M. Ulibarri, D. Vaniman, N. Warner, R. Waterbury, R. Whitaker, J. Witt, B. Wong-Swanson, The ChemCam instrument suite on the Mars Science Laboratory (MSL) rover: Body unit and combined system tests. *Space Sci. Rev.* **170**, 167–227 (2012). doi:10.1007/s11214-012-9902-4
64. D. F. Blake, R. V. Morris, G. Kocurek, S. M. Morrison, R. T. Downs, D. Bish, D. W. Ming, K. S. Edgett, D. Rubin, W. Goetz, M. B. Madsen, R. Sullivan, R. Gellert, I. Campbell, A. H. Treiman, S. M. McLennan, A. S. Yen, J. Grotzinger, D. T. Vaniman, S. J. Chipera, C. N. Achilles, E. B. Rampe, D. Sumner, P. Y. Meslin, S. Maurice, O. Forni, O. Gasnault, M. Fisk, M. Schmidt, P. Mahaffy, L. A. Leshin, D. Glavin, A. Steele, C. Freissinet, R. Navarro-González, R. A. Yingst, L. C. Kah, N. Bridges, K. W. Lewis, T. F. Bristow, J. D. Farmer, J. A. Crisp, E. M. Stolper, D. J. Des Marais, P. Sarrazin, C. Agard, J. A. Alves Verdasca, R. Anderson, R. Anderson, D. Archer, C. Armiens-Aparicio, R. Arvidson, E. Atlaskin, S. Atreya, A. Aubrey, B. Baker, M. Baker, T. Balic-Zunic, D. Baratoux, J. Baroukh, B. Barraclough, K. Bean, L. Beegle, A. Behar, J. Bell, S. Bender, M. Benna, J. Bentz, G. Berger, J. Berger, D. Berman, J. J. Blanco Avalos, D. Blaney, J. Blank, H. Blau, L. Bleacher, E. Boehm, O. Botta, S. Bottcher, T. Boucher, H. Bower, N. Boyd, B. Boynton, E. Breves, J. Bridges, W. Brinckerhoff, D. Brinza, C. Brunet, A. Brunner, W. Brunner, A. Buch, M. Bullock, S. Burmeister, M. Cabane, F. Calef, J. Cameron, B. Cantor, M. Caplinger, J. C. Rodriguez, M. Carmosino, I. C. Blazquez, A. Charpentier, D. Choi, B. Clark, S. Clegg, T. Cleghorn, E. Cloutis, G. Cody, P. Coll, P. Conrad, D. Coscia, A. Cousin, D. Cremers, A. Cros, F. Cucinotta, C. d'Uston, S. Davis, M. Day, M. T. Juarez, L. DeFlores, D. DeLapp, J. DeMarines, W. Dietrich, R. Dingler, C. Donny, D. Drake, G. Dromart, A. Dupont, B. Duston, J. Dworkin, M. D. Dyar, L. Edgar, C. Edwards, L. Edwards, B. Ehlmann, B. Ehresmann, J. Eigenbrode, B. Elliott, H. Elliott, R. Ewing, C. Fabre, A. Fairen, K. Farley, C. Fassett, L. Favot, D. Fay, F. Fedosov, J. Feldman, S. Feldman, M. Fitzgibbon, G. Flesch, M. Floyd, L. Fluckiger, A. Fraeman, R. Francis, P. Francois, H. Franz, K. L. French, J. Frydenvang, A. Gaboriaud, M. Gailhanou, J. Garvin, C. Geffroy, M. Genzer, A. Godber, F. Goesmann, D. Golovin, F. G. Gomez, J. Gomez-Elvira, B. Gondet, S. Gordon, S. Gorevan, J. Grant, J. Griffes, D. Grinspoon, P. Guillemot, J. Guo, S. Gupta, S. Guzewich, R. Haberle, D. Halleaux, B. Hallet, V. Hamilton, C. Hardgrove, D. Harker, D. Harpold, A.-M. Harri, K. Harshman, D. Hassler, H. Haukka, A. Hayes, K. Herkenhoff, P. Herrera, S. Hettrich, E. Heydari, V. Hipkin, T. Hoehler, J. Hollingsworth, J. Hudgins, W. Huntress, J. Hurowitz, S. Hviid, K. Iagnemma, S. Indyk, G. Israel, R. Jackson, S. Jacob, B. Jakosky, E. Jensen, J. K. Jensen, J. Johnson, M. Johnson, S. Johnstone, A. Jones, J. Jones, J. Joseph, I. Jun, H. Kahanpaa, M. Kahre, N. Karpushkina, W. Kasprzak, J. Kauhanen, L. Keely, O. Kemppinen, D. Keymeulen, M.-H. Kim, K. Kinch, P. King, L. Kirkland, A. Koefoed, J. Kohler, O. Kortmann, A. Kozyrev, J. Krezoski, D. Krysak, R. Kuzmin, J. L. Lacour, V. Lafaille, Y. Langevin, N. Lanza, J. Lasue, S. Le Mouelic, E. M. Lee, Q.-M. Lee, D. Lees, M. Lefavor, M. Lemmon, A. Lepinette Malvitte, R. Leveille, E. Lewin-Carpintier, S. Li, L. Lipkaman, C. Little, M. Litvak, E. Lorigny, G. Lugmair, A. Lundberg, E. Lyness, J. Maki, A. Malakhov, C. Malespin, M. Malin, N. Mangold, H. Manning, G. Marchand, M. Marin Jimenez, C. Martin Garcia, D. Martin, M. Martin, J. Martinez-Frias, J. Martin-Soler, F. J. Martin-Torres, P. Mauchien, A. McAdam, E. McCartney, T. McConnochie, E. McCullough, I. McEwan, C. McKay, S. McNair, N. Melikechi, M. Meyer, A. Mezzacappa, H. Miller, K. Miller, R. Milliken, M. Minitti, M. Mischna, I. Mitrofanov, J. Moersch, M. Mokrousov, A. Molina Jurado, J. Moores, L. Mora-Sotomayor, J. M. Morookian, R. Mueller-Mellin, J.-P. Muller, G. Munoz Caro, M. Nachon, S. Navarro Lopez, K. Nealson, A. Nefian, T. Nelson, M. Newcombe, C. Newman, H. Newsom, S. Nikiforov, P. Niles, B. Nixon, E. N. Dobrea, T. Nolan, D. Oehler, A. Ollila, T. Olson, T. Owen, H. Pablo, A. Paillet, E. Pallier, M. Palucis, T. Parker, Y. Parot, K. Patel, M. Paton, G. Paulsen, A. Pavlov, B. Pavri, V. Peinado-Gonzalez, R. Pepin, L. Peret, R. Perez, G. Perrett, J. Peterson, C. Pilorget, P. Pinet, J. Pla-Garcia, I. Plante, F. Poitrasson, J. Polkko, R. Popa, L. Posiolova, I. Pradler, B. Prats, V. Prokhorov, S. W. Purdy, E. Raaen, L. Radziemski, S. Rafkin, M. Ramos, F. Raulin, M. Ravine, G. Reitz, N. Renno, M. Rice, M. Richardson, F. Robert, J. A. Rodriguez Manfredi, J. J. Romeral-Planello, S. Rowland, M. Saccoccio, A. Salamon, J. Sandoval, A. Sanin, S. A. Sans Fuentes, L. Saper,

V. Sautter, H. Savijarvi, J. Schieber, W. Schmidt, D. Scholes, M. Schoppers, S. Schroder, E. Sebastian Martinez, A. Sengstacken, R. Shterts, K. Siebach, T. Siili, J. Simmonds, J.-B. Sirven, S. Slavney, R. Sletten, M. Smith, P. Sobron Sanchez, N. Spanovich, J. Spray, S. Squyres, K. Stack, F. Stalport, T. Stein, J. Stern, N. Stewart, S. L. S. Stipp, K. Stoiber, B. Sucharski, R. Summons, V. Sun, K. Supulver, B. Sutter, C. Szopa, C. Tate, S. Teinturier, I. L. ten Kate, P. Thomas, L. Thompson, R. Tokar, M. Toplis, J. Torres Redondo, M. Trainer, V. Tretyakov, R. Urqui-O'Callaghan, J. Van Beek, T. Van Beek, S. VanBommel, A. Varenikov, A. Vasavada, P. Vasconcelos, E. Vicenzi, A. Vostrukhin, M. Voytek, M. Wadhwa, J. Ward, C. Webster, E. Weigle, D. Wellington, F. Westall, R. C. Wiens, M. B. Wilhelm, A. Williams, J. Williams, R. Williams, R. B. Williams, M. Wilson, R. Wimmer-Schweingruber, M. Wolff, M. Wong, J. Wray, M. Wu, C. Yana, C. Zeitlin, R. Zimdar, M.-P. Zorzano Mier; MSL Science Team, Curiosity at Gale Crater, Mars: Characterization and analysis of the Rocknest sand shadow. *Science* **341**, 1239505 (2013). doi:10.1126/science.1239505 Medline

65. H. W. Nesbitt, R. E. Wilson, Recent chemical weathering of basalts. *Am. J. Sci.* **292**, 740–777 (1993). doi:10.2475/ajs.292.10.740
66. J. L. Campbell, G. M. Perrett, R. Gellert, S. M. Andrushenko, N. I. Boyd, J. A. Maxwell, P. L. King, C. D. M. Schofield, Calibration of the Mars Science Laboratory alpha particle x-ray spectrometer. *Space Sci. Rev.* **170**, 319–340 (2012). doi:10.1007/s11214-012-9873-5
67. L. M. Thompson *et al*., BT-2 calibration target for the Mars Science Laboratory alpha particle x-ray spectrometer: Characterization and alkali basalt Martian analogue. *Lunar Planet. Sci. Conf.* 44, Abstract 2190 (2013).
68. R. Gellert, R. Rieder, J. Brückner, B. C. Clark, G. Dreibus, G. Klingelhöfer, G. Lugmair, D. W. Ming, H. Wänke, A. Yen, J. Zipfel, S. W. Squyres, Alpha particle x-ray spectrometer (APXS): Results from Gusev Crater and calibration report. *J. Geophys. Res. Planets* **111**, E02S05 (2006). doi:10.1029/2005JE002555
69. R. C. Wiens *et al.*, Pre-flight calibration and initial data processing for the ChemCam laser-induced breakdown spectroscopy instrument on the Mars Science Laboratory rover. *Spectrochim. Acta [A]* **B82**, 1–27 (2013).
70. S. M. Clegg *et al*., Quantitative remote laser induced breakdown spectroscopy by multivariate analysis. *Spectrochim. Acta [A]* **B64**, 79–88 (2009).
71. S. Le Mouelic *et al*., Mars imaging by the ChemCam remote microscopic imager (RMI) onboard Curiosity: The first three months. *Lunar Planet. Sci. Conf.* **44**, Abstract 1213 (2013).
72. M. H. Reed *et al*., *Users Guide for CHIM-XPT* (University of Oregon, 2010).

**Acknowledgments:** Much of this research was carried out at the Jet Propulsion Laboratory, California Institute of Technology, under contract with NASA. Development and operation of the ChemCam and APXS instruments were also supported by funds from the French Space Agency, CNES, and the Canadian Space Agency. Organizations supporting research include NASA, the Canadian Space Agency, NSERC (Canada), and the United Kingdom Space Agency (UK). Chemical data presented here are derived from archived data sets in the NASA Planetary Data System (PDS) http://pds-geosciences.wustl.edu/missions/msl. We are grateful to the MSL engineering and management teams for making the mission and this scientific investigation possible and to science team members who contributed to mission operations. The senior author (S.M.M.) thanks Lamont-Doherty Earth Observatory of Columbia University, and especially S. Hemming, for hospitality during a sabbatical when the manuscript was being prepared.

**Supplementary Materials**

www.sciencemag.org/cgi/content/full/science.1244734/DC1
Materials and Methods
Figs. S1 to S8
Tables S1 to S8
MSL Science Team Author List
References (*66–72*)

15 August 2013; accepted 12 November 2013
Published online 9 December 2013
10.1126/science.1244734

**Author Affiliations**

[1]Department of Geosciences, State University of New York at Stony Brook, Stony Brook, NY, 11794-2100, USA. [2]U.S. Geological Survey, Astrogeology Science Center, Flagstaff, AZ 86001, USA. [3]School of Earth and Space Exploration, Arizona State University, Tempe, AZ 85287, USA. [4]Space Research Centre, Department of Physics and Astronomy, University of Leicester LE1 7RH, UK. [5]Jet Propulsion Laboratory, California Institute of Technology, Pasadena, CA 91109, USA. [6]Department of Physics, University of Guelph, Guelph, ON, N1G 2W1, Canada. [7]Space Science Institute, Boulder, CO, USA. [8]Chemistry Division, Los Alamos National Laboratory, Los Alamos, NM, 87545, USA. [9]NASA Goddard Space Flight Center, Greenbelt, MD 20771, USA. [10]Department of Space Sciences, NASA Ames Research Center, Moffett Field, CA 91109, USA. [11]Laboratoire de Geologié de Lyon, Université de Lyon, 69364 Lyon, France. [12]Department of Astronomy, Mt. Holyoke College, South Hadley, MA 01075, USA. [13]Division of Geological and Planetary Sciences, California Institute of Technology, Pasadena, CA 91125, USA. [14]UMR 7359 CNRS-Georesources, Campus des Aiguillettes, Faculté des Sciences, BP 70239, 54506 Vandoeuvre Les Nancy, Cedex, France. [15]IRAP, Université de Toulouse (UPS-OMP)/CNRS, 9, Avenue du Colonel Roche, BP 44346, 31028 Toulouse, Cedex 4, France. [16]Institute of Meteoritics, University of New Mexico, Albuquerque, NM 87131, USA. [17]Center for Earth and Planetary Sciences, National Air and Space Museum, Smithsonian Institution, 6th at Independence SW, Washington, DC 20560, USA. [18]Department of Earth Science and Engineering, Imperial College London, London, SW7 2AZ, UK. [19]Research School of Earth Sciences, Australian National University, Canberra, ACT, 0200, Australia. [20]Laboratoire de Planétologie et Géodynamique, LPGN/CNRS UMR 6112 and Université de Nantes, 4432 Nantes, France. [21]School of Science, Rensselaer Polytechnic Institute, Troy, NY 12180, USA. [22]Canadian Space Agency, St.-Hubert, QC, J3Y 8Y9, Canada. [23]Princeton University, Princeton, NJ 08544, USA. [24]Observatoire Midi-Pyrenees, Toulouse, France. [25]NASA Johnson Space Center, Houston, TX 77058, USA. [26]Department of Earth Sciences, Brock University, St. Catherines, ON L2S 3A1, Canada. [27]CEPSAR, Open University, Milton Keynes MK7 6AA, UK. [28]Department of Earth and Planetary Sciences, University of California, Davis, CA 95616, USA. [29]Lunar Planetary Science Institute, Houston, TX 77058, USA. [30]Planetary Science Institute, Tucson, AZ, 85719, USA. [31]International Space and Response Division, Los Alamos National Laboratory, Los Alamos, NM, 87545, USA.

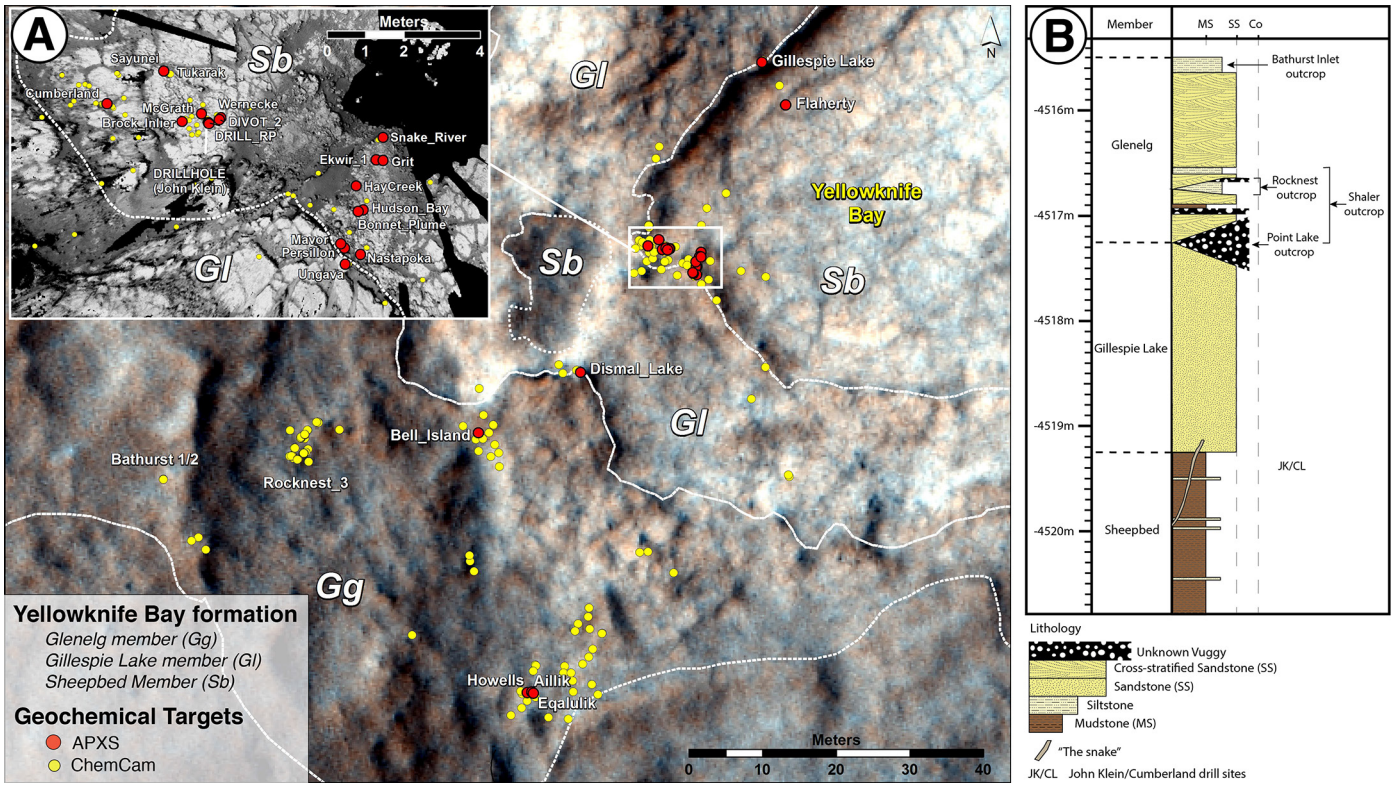


**Fig. 1. Geological context and locations of analyses.** (**A**) HiRISE image (part of PSP_010573_1755) showing geological relationships of the Yellowknife Bay formation, location and names of APXS analyses, locations of ChemCam LIBS analyses, and names of ChemCam targets, Tukarak and McGrath (also an APXS target), discussed in the text. The inset shows expanded Navigational camera overhead projection of the region where drilling of the Sheepbed member took place (John_Klein and Cumberland) and where the Selwyn Section (targets between Snake_River and Ungava) was examined. Additional details about sample locations, including the ChemCam target names, are shown in figs. S1 to S7. (**B**) Stratigraphic section of the Yellowknife Bay formation at Yellowknife Bay. Also shown is the stratigraphic relationship of the cross-cutting dike-like feature termed "the snake" [adapted from (*2*)].

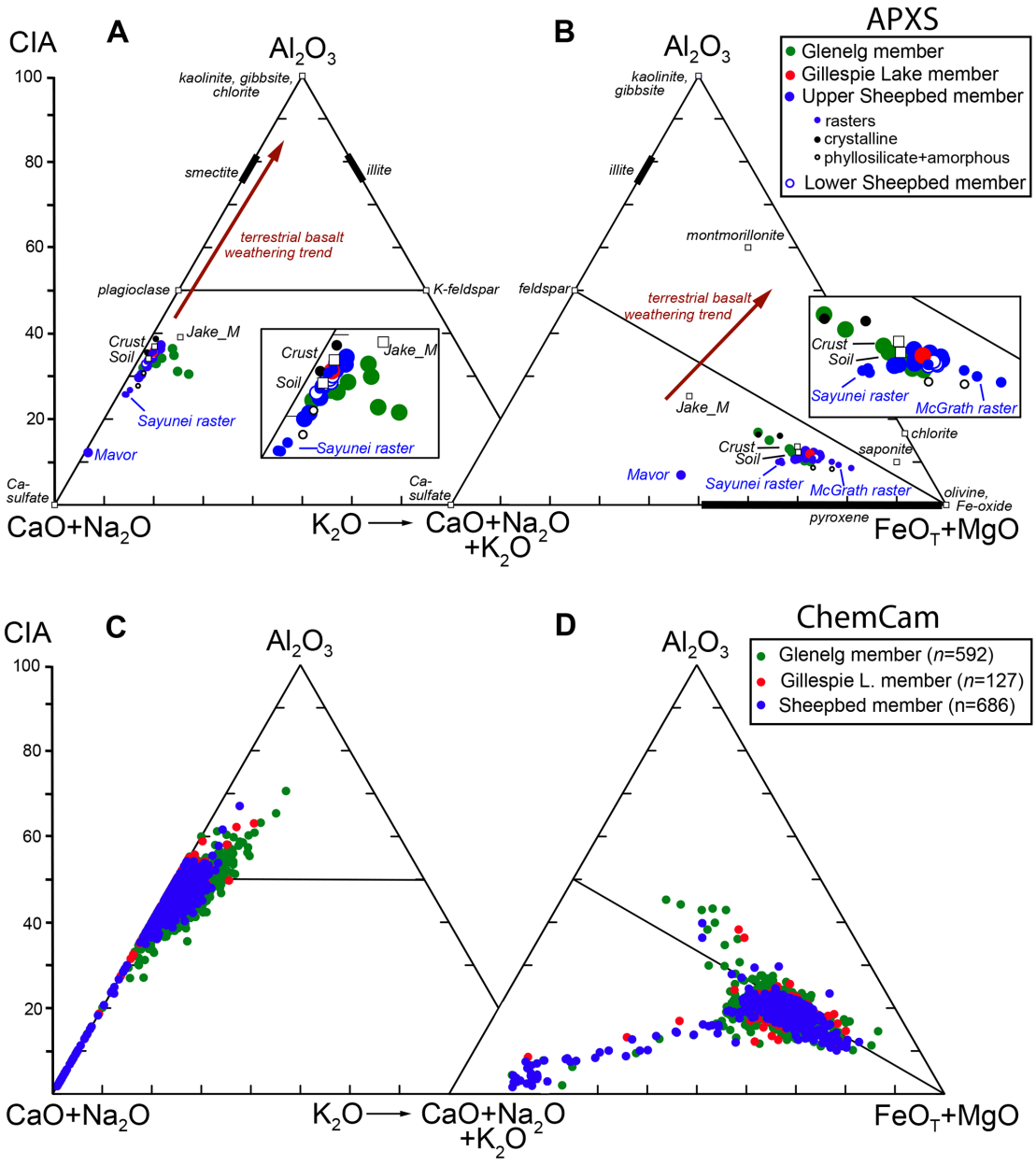


**Fig. 2. $Al_2O_3$–($CaO+Na_2O$)–$K_2O$ and $Al_2O_3$–($CaO+Na_2O+K_2O$)–($FeO_T+MgO$) ternary diagrams.** (**A** and **B**) APXS data; (**C** and **D**) ChemCam data. Shown for reference are the CIA scale [measured on (A) and (C) only], and, as open squares, average Martian crust (*12*), local soil (*64*), and the local rock Jake_Matiijevic (Jake_M) (*45*), modeled compositions of John_Klein and Cumberland crystalline and clay+amorphous materials (*4*), and arrows representing typical trends observed for terrestrial weathering profiles on basalts (*65*). The insets of (A) and (B) are expanded views of the main cluster of data.

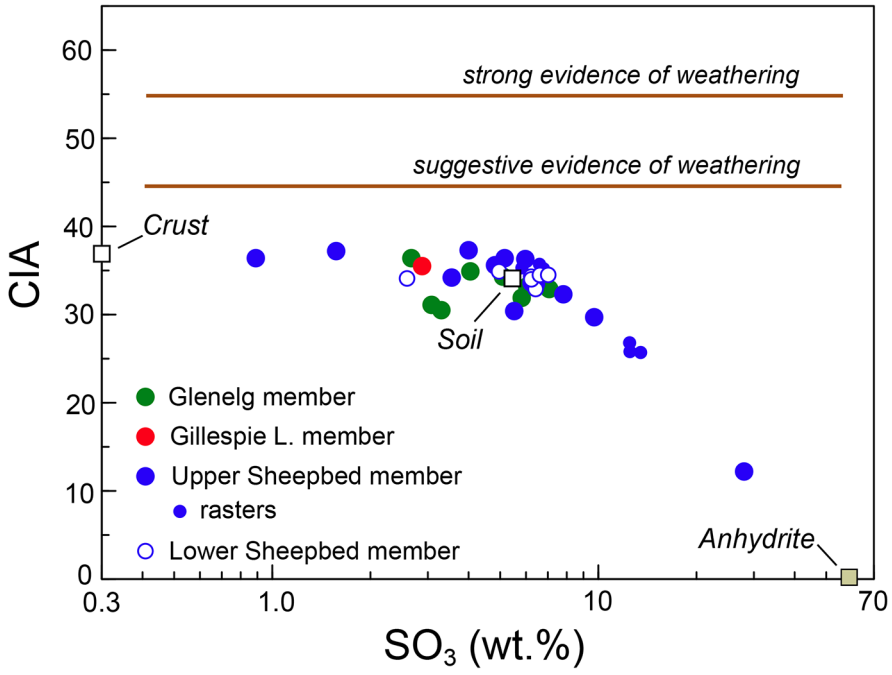


**Fig. 3. Plot of CIA versus $SO_3$ contents for Yellowknife Bay formation APXS analyses.** Shown for reference, as open squares, are average Martian crust (*12*), local soil (*64*), the composition of anhydrite ($CaSO_4$) and horizontal lines that show the CIA values expected for basaltic sedimentary rocks that have experienced a chemical weathering history.

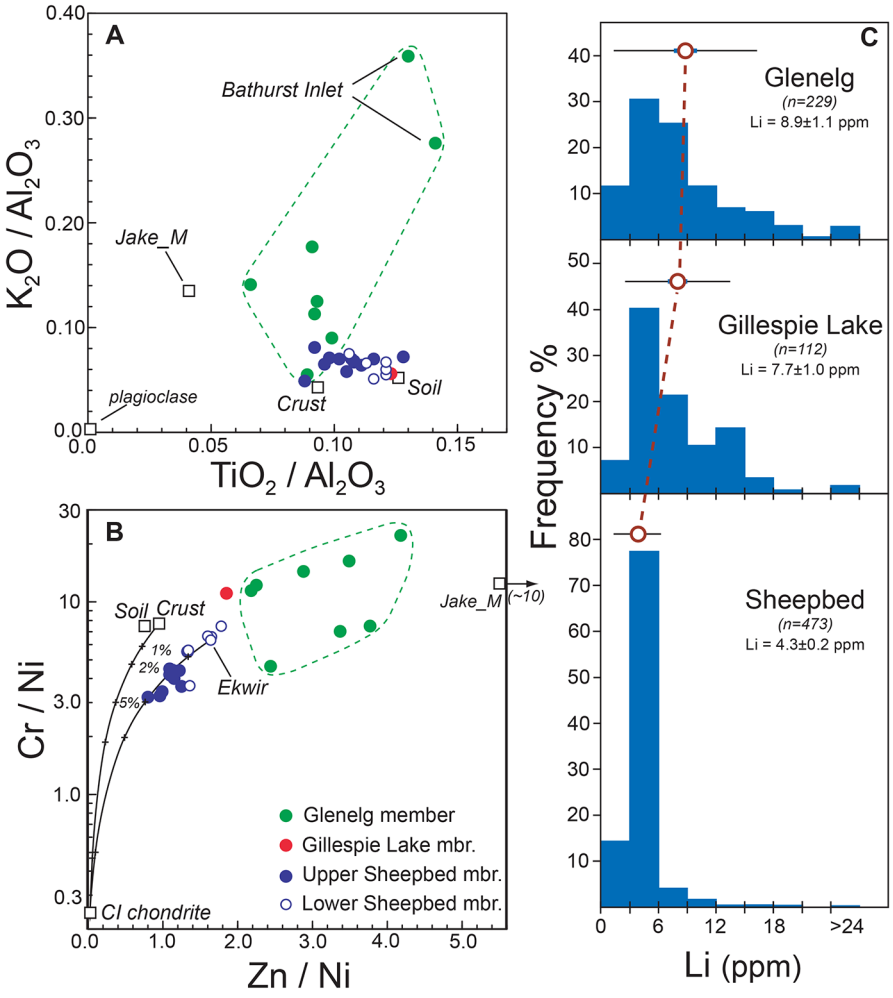


**Fig. 4. Geochemical relationships within the Yellowknife Bay formation highlighting stratigraphic variations.** (**A**) APXS $K_2O/Al_2O_3$ versus $TiO_2/ Al_2O_3$; (**B**) APXS Cr/Ni versus Zn/Ni; (**C**) histograms of ChemCam Li abundances also showing mean (red circle), standard deviation (black bar) and 95% confidence interval (blue bar; also the uncertainty reported on the averages). In Fig. 4, A and B, the compositions of average Martian crust (*12*), local soil (*64*), the rock Jake_Matijevic (*45*), average CI chondrite (*12*) and plagioclase are shown for reference. Also shown on Fig. 2B are mixing lines between average Martian crust and the Ekwir_Brush target and average CI chondrite.

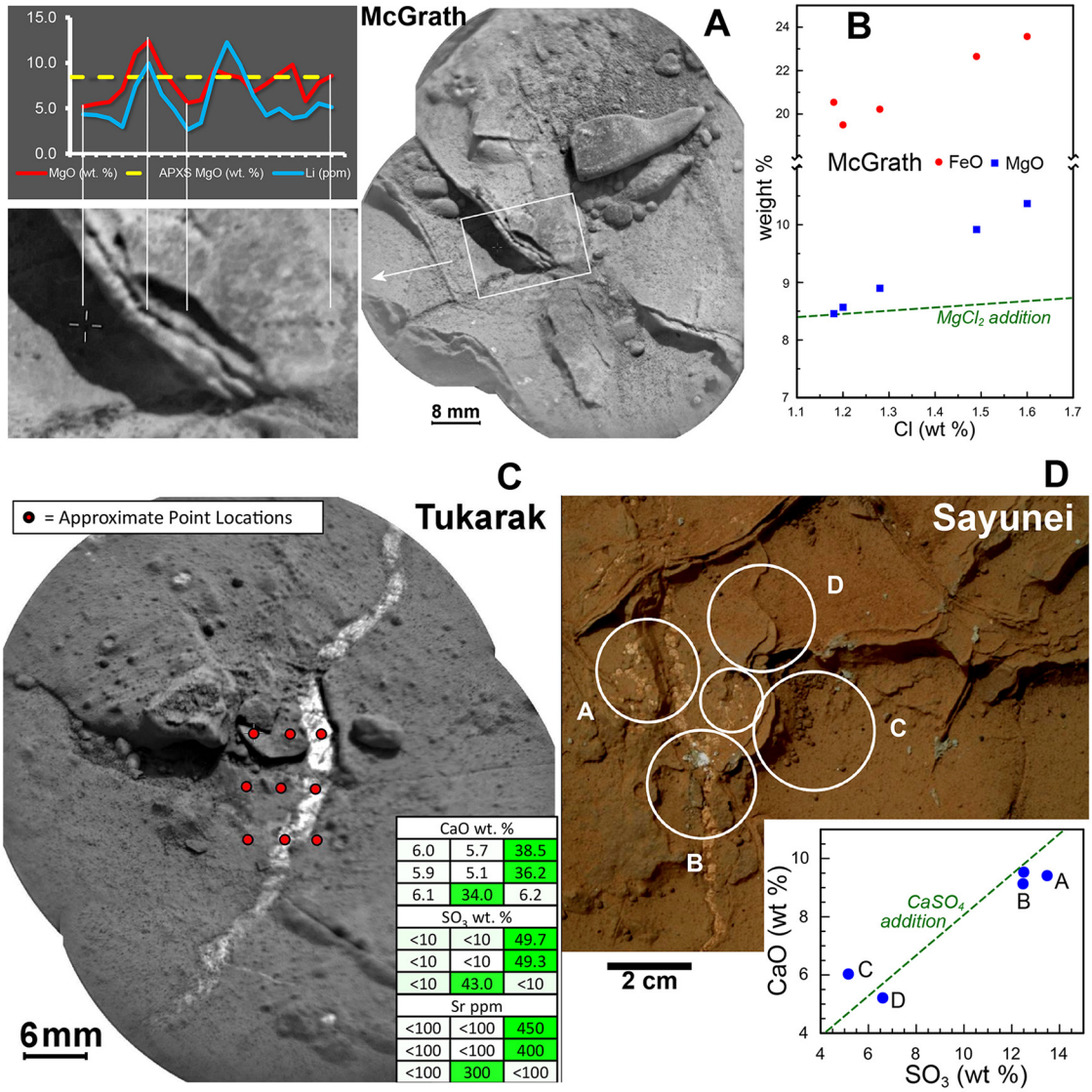


**Fig. 5. Geochemical constraints on diagenetic features within the Yellowknife Bay formation.** (**A**) ChemCam RMI image of the McGrath target "raised ridge" that is dipping gently to the upper right. The inset shows LIBS MgO and Li transects for 20 shots taken a cross the feature. Shown for reference is the average MgO of McGrath, determined by APXS. Note elevated and correlated Mg and Li at the site of the raised ridge. Also note that elevated Mg (but not Li) is observed on the right hand side that likely represents the outer layer of the cement, exposed on the dipping surface. (**B**) APXS raster analysis for McGrath showing elevated Fe and Mg that correlate with Cl. Note the break in the scale on the y-axis. A model of $MgCl_2$ addition is shown to illustrate that the correlation is not due simply to the presence of chloride phases. (**C**) ChemCam RMI image of a late diagenetic light-toned fracture at the Tukarak target. Location of a 3x3 LIBS raster is shown and results for Ca, S and Sr, relative to their position in the raster, are given in the inset table. (**D**) APXS raster analysis on late diagenetic light-toned fracture at the Sayunei target. The inset shows the plot of CaO versus $SO_3$, with a model illustrating the effects of $CaSO_4$ addition.

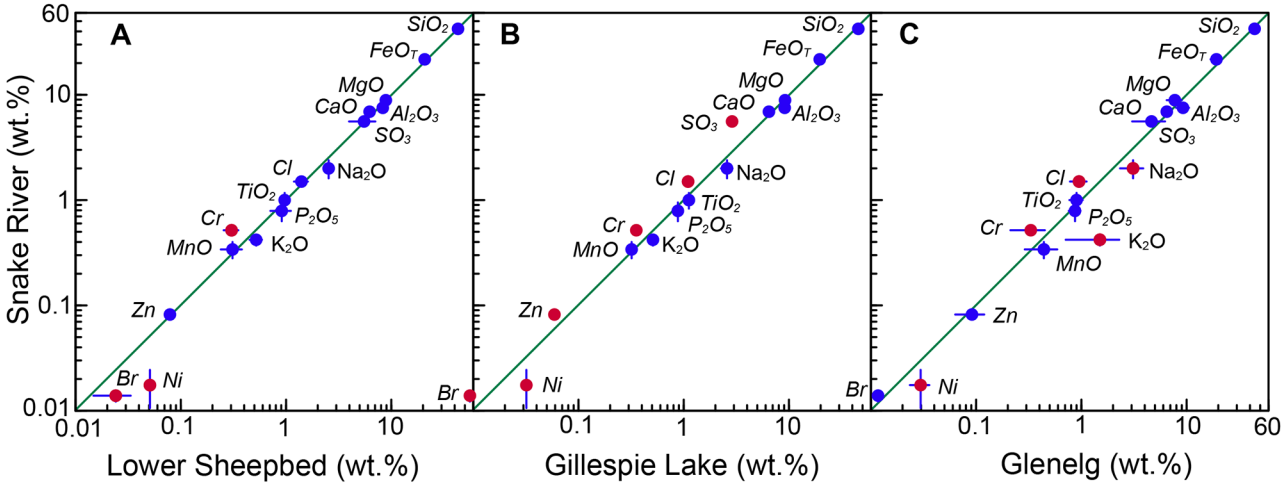


**Fig. 6. Comparison diagrams for the dike-like feature, termed the "snake".** APXS composition of the Snake_River target compared to (**A**) lower Sheepbed member average, (**B**) Gillespie Lake member sample and (**C**) Glenelg member average. The upper Sheepbed is not used for this comparison because compared to the lower Sheepbed, its geochemistry is more heavily influenced by diagenetic features (e.g., Ca-sulfate veins, concretions). The diagonal green line represents equal compositions. Error bars (if larger than the symbol size) represent two sigma errors for individual samples (Snake_River, Gillespie Lake) and one standard deviation on the mean for averages (Lower Sheepbed member, Glenelg member). Significant differences in composition are shown as red symbols.